2012

Experimental Investigation of Particulate Deposition on a Simulated Film-Cooled Turbine Vane Pressure Surface in a High Pressure Combustion Facility

Robert G. Murphy
West Virginia University

Experimental Investigation of Particulate Deposition on a Simulated Film-Cooled Turbine Vane Pressure Surface in a High Pressure Combustion Facility

Robert G. Murphy

Thesis submitted to the
Benjamin M. Statler College of Engineering and Mineral Resources
at West Virginia University
in partial fulfillment of the requirements
for the degree of

Master of Science
in
Mechanical Engineering

Andrew C. Nix, Ph.D., Chair
Gary Morris, Ph.D.
Edward Sabolsky, Ph.D.
Seth A. Lawson, Ph.D.

Department of Mechanical and Aerospace Engineering

Morgantown, West Virginia
2012

Keywords: Gas Turbines; Film Cooling; Deposition

ABSTRACT

Experimental Investigation of Particulate Deposition on a Simulated Film-Cooled Turbine Vane Pressure Surface in a High Pressure Combustion Facility

Robert G. Murphy

Use of coal syngas for Integrated Gasification Combined Cycle (IGCC) industrial gas turbines introduces contaminants into the flow that can deposit onto the components of the first stage of the turbine. These deposit structures may create alterations in the cooling scheme and can erode or react with thermal barrier coatings (TBC). A study was performed to examine the evolution and contributing factors to the growth of deposit structures in a simulated gas turbine environment. Tests were performed in the high pressure/temperature aerothermal facility at the Department of Energy's (DoE) National Energy Technology Laboratory (NETL) in Morgantown, WV. The facility was operated at a pressure of 45 psig and temperatures ranging from 1950^{o}F to 2350^{o}F. Two test article geometries with four film cooling holes non-dimensionally matched to a large-scale industrial gas turbine were created to simulate the pressure side of a first stage vane. A high pressure seeding system was developed to inject coal fly-ash to simulate the build-up of particulate matter experienced by industrial gas turbines into the high pressure facility to perform accelerated deposition of the fly-ash onto the test articles. A method was developed to process the fly-ash to match the theoretical size distribution and particle flow dynamics representative of an industrial gas turbine scaled. Analyses were performed to determine whether the particles reached thermal equilibrium before impacting the test article and to estimate the penetration depth of the particles from the injection tube into the mainstream flow of the facility cross flow. Five independent variable effects were studied; impaction angle, freestream temperature, blowing ratio, surface (TBC or no TBC), and increases in simulated operating hours. In studying the effects of surface impaction angle, deposition

increased as the face angle of the test article increased from 10^{o} to 20^{o}. Variation of the freestream temperature showed that the deposition was dependent on a theoretical sticking freestream temperature of 2315^{o}F. Deposition resisted forming at temperatures below the theoretical sticking temperature. In studying the effects of blowing ratio, deposition formation increased as the blowing ratio (mass flux of cooling flow/mass flux of the mainstream flow) decreased from M=1.0, 0.25 and finally to 0.0 (no cooling). The study of the effects of the surface coating on deposition showed that TBC's increased the rate of deposition over the exact same test article that was not coated. Instead of forming new deposits with twice the run time, the deposits started forming on top of other deposits showing that even at high particulate loadings the deposition did not affect the film cooling downstream of the cooling holes. Post test surface roughness scans were planned and performed on the test articles that didn't have deposits break off as they were removed from the facility. Most test articles were not scanned due to the flyash deposits breaking or "sluffing" off as the test article cooled after the conclusion of the test. In contrast, the flyash deposits that formed on the interior (non-TBC coated) walls of the test section did not display any sluffing during cool down. This research is valuable to gas turbine manufacturers and operators to understand the variables that promote deposition so appropriate mitigations can be put in place to prevent engine downtime and component failures.

TABLE OF CONTENTS

LIST OF FIGURES

LIST OF TABLES

NOMENCLATURE

A_s	particle surface area
c_o	speed of light in a vacuum ($c_o = 2.998 \times 10^8$ m/s)
c_p	specific heat
d_c	cooling hole diameter
d_p	particle diameter
$d_{p,med}$	median particle diameter
d_{tube}	diameter of injection tubing
h	heat transfer coefficient
h_p	Planck constant ($h_p = 6.626 \times 10^{-34}$ J-s)
I_1	Total Surface Intensity of the bare metal in the trench
I_2	Total Surface Intensity of the Thermal Barrier Coating (TBC)
I_{BB}	Emitted Intensity of the face (Assumed to be the same everywhere on the face)
I_W	Emitted Reflective Intensity of the surrounding walls (Assumed to be the same across the face of the coupon)
k	Boltzmann constant ($k = 1.381 \times 10^{-23}$ J/K)
k_f	thermal conductivity of the fluid
M	blowing ratio, $\rho_c (U_c)/\rho_\infty (U_\infty)$
N	number of points in profile record
Nu_d	Nusselt number based on particle diameter length scale
Pr	Prandtl number
Ra	centerline averaged roughness
Re_c	Reynolds number based on cooling hole diameter length scale
Re_d	Reynolds number based on particle diameter length scale
Rq	root mean square roughness
Rt	peak-to-valley roughness
Sra, R_a	centerline average roughness
SRp	distance from highest peak to centerline roughness
SRq, R_q	root mean squared average roughness height
SRv	distance from lowest valley to centerline roughness
SRz	mean peak-to-valley height
St	Stanton number
Stk	median Stokes number
t	time
T_∞	freestream temperature
T_i	particle initial temperature
T_p	particle temperature
T_s	surface temperature
U_∞	freestream velocity
U_c	coolant (nitrogen) gas velocity
U_p	velocity of particle
V	particle volume
y_i	surface height compared to mean surface height
Y_{max}	maximum penetration depth
Y_{mid}	penetration at the maximum mass fraction
Y_{min}	minimum penetration depth

Z	distance downstream of the injection point using the center of the injection hole as a reference

Greek

ε_1	Emissivity of the bare metal in the trench
ε_2	Emissivity of the TBC
λ	wavelength (λ = 900nm = 9 x 10^{-7} m)
μ_∞	freestream gas dynamic viscosity
ρ_∞	freestream gas density
ρ_c	coolant (nitrogen) gas density
ρ_p	particle density
υ_∞	freestream gas kinematic viscosity
τ	transmissivity of optics
τ_f	time characteristic of the flow
τ_p	settling time characteristic of the particle

ACKNOWLEDGEMENTS

First I would like to thank the members of my committee for their support. Dr. Gary Morris is an excellent instructor and undergraduate advisor whose guidance I appreciated to guide me into my graduate career. I never had the pleasure of having Dr. Edward Sabolsky in class but he runs the finest fantasy football league in the MAE department which I was lucky enough to win in 2010.

I would like to extend my thanks to Dr. Klaus Brun, Andrea Barnett and the rest of the staff at the Southwest Research Institute for selecting me as a 2011 University Turbine Systems Research Fellow and placing me at Solar Turbines, Inc. While at Solar I had tremendous guidance from Dr. Yong Kim of the Heat Transfer Group. The projects he had me work on both challenged me and allowed me to grow in the heat transfer field. I would like to thank John Mason, Dr. Hee-Koo Moon, Charmaine Gary, my fellow interns, and rotational engineers for all of their support during my time at Solar that allowed me to perform well and be offered a permanent position at the end of my Masters work.

The Oak Ridge Alliance of Universities for selecting me an Oak Ridge Institute for Science and Education Fellow to work in a government setting at the Department of Energy's National Energy Technology Laboratory. Thanks to Todd Sidwell, Kent Castleton, Steve Beers, and Clint Beddick for their support on this project. I would like to give special thanks to Jeff Riley and Mark Tucker for being the best two technicians (and most entertaining to work with) any engineer could ever ask for. Their hard work and creative problem solving helped save an enormous amount of time. This dedication, for which I am truly grateful, allowed us to get the maximum amount of runs in that could possibly be completed in the allotted time. Finally, I would like to thank my ORISE mentor Doug Straub for teaching me how to work in a

government setting and for providing me with good projects to complete and learn from. I also want to thank him for sending off the well timed and politely strong email from time to time to help “unclog” the government required processes to move the project along.

Thanks to my friend and colleague Dr. Seth A. Lawson. Thanks for all of the help in working through the issues we had during this project. Your knowledge and experience (and insanely positive attitude) really helped me work through the ups and downs of this project. I appreciated all of your help in paper and proposal writing and preparation of proposals.

A special thank you to my advisor Dr. Andrew C. Nix. Thank you for introducing me into a field that I enjoy working in everyday. Thanks for expanding my contacts, taking me to conferences, giving me the opportunity to write papers and proposals and letting me experience as much as possible in the gas turbine field during my time at WVU. You gave me the opportunity to learn as much about the field outside of the lab as I did in it.

Finally, thank you to my friends and especially my family. The best thing I can say is that I am who I am today thanks to all of the experiences and love that you have given me over the years. I am forever grateful for the support.

CHAPTER 1:
Introduction

A gas turbine is essentially a power plant that produces a large power density. Air is ingested into the compressor where the pressure and temperature are elevated. At the exit of the compressor the air moves into the combustor where fuel is added and combustion occurs resulting in a temperature increase. The exhaust gases that leave the combustor exit directly onto the first stage turbine vanes. An image of an industrial gas turbine setup is shown in Figure 1.1.

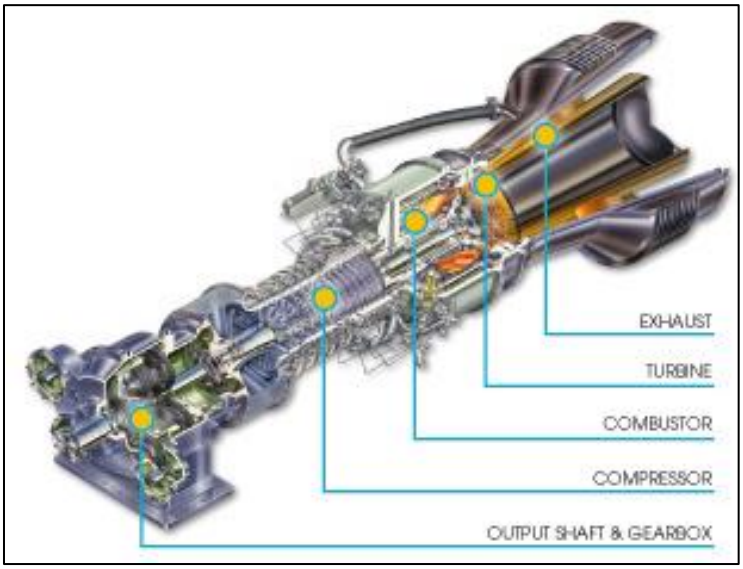

Figure 1.1. Image of a Solar Turbines, Inc. Titan 130 single shaft gas turbine for power generation applications[1]**.**

Conditions at the exit of the combustor of an industrial gas turbine are some of the harshest conditions that can be experienced by any machine. The first stage of the turbine section is exposed to these extremely high temperatures and pressures. Since 1950, the firing temperatures of gas turbines have increased by more than 1100 ^{o}F to over 2500^{o}F[5]. During the same period pressure ratios have increased from around 10 to over 35. The reason for the continuing increase in pressures and temperatures is that the higher these values rise the more

power can be produced and higher thermal efficiency can be achieved. The main limiting factor when increasing the firing temperature is the materials and cooling schemes used to protect the blades and vanes. The current firing temperature levels in industrial gas turbines are above the melting temperature of the metals used to manufacture components, requiring advanced materials and cooling schemes. To combat this issue new materials and cooling schemes will be needed. As the temperatures rise, understanding the heat transfer issues that accompany the rise is paramount to a long successful engine life.

To combat the harsh conditions, film-cooling is one of the types of cooling used to help protect the blade. The cooling air for film-cooled components is extracted from the high pressure compressor and routed around the combustor. This air is then injected into the turbine vomponents where it cools the inside of the blades and vanes before being injected back into the core flow through holes on the exterior of the blades and vanes to form a thin "film" to protect the face of the component and lower the surface temperature and protect the component. It is important to note that cooling air is at an elevated temperature but is much lower than the temperature of the core flow exiting the combustor. Figure 1.2 displays a film-cooled and internally cooled turbine vane.

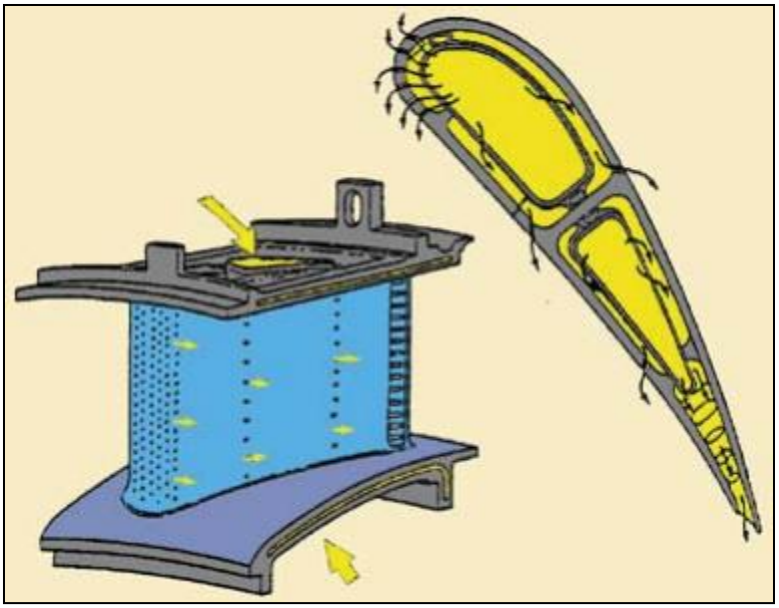

Figure 1.2. Film-cooled turbine vane[2]**.**

Film-cooling schemes are designed for new components that have smooth surfaces that have not been subjected to hours of operation that increase the surface roughness. However, the use of alternative fuels, such as coal-derived synthesis gas (syngas) in modern integrated gasification combined cycle (IGCC) gas turbine engines has introduced contaminants into the flow that can potentially damage components of the engine by increasing surface roughness, which affects aerodynamics, increases HT coefficient and reduces cooling effectiveness. Even with modern filtration systems, contaminant particles smaller than 10 μm will pass through the filters and into the engine [6]. As the filters wear out larger particles may pass through. The particles will pass through the combustor and be heated until they are in molten form. As these molten particles impact the components in the first stage of the turbine, they will deposit on turbine airfoil components. The growth of deposition may disrupt the film-cooling scheme, and in some cases completely cover the holes as seen in Figure 1.3. This issue can also be caused by other situations such as the ingestion of volcanic ash in an aviation gas turbine. Once the film-cooling scheme is disrupted the blade will start to develop hot spots and will eventually fail.

Figure 1.3. Film-cooled turbine vane covered by particulate matter[3]**.**

Understanding the evolution of the deposits and their effects on cooling schemes and heat transfer of the first stage vanes and blades is crucial to extending the life of engine components and reducing down time. The process of deposition and build up of deposits occurs over thousands of hours of engine operation, which complicates experimental testing. In order to investigate the effects of particulate deposits on film cooling in a lab environment, the process of deposition must be accelerated. Accelerated deposition will be discussed in detail in Chapter 2 however the concept is that the particulate loading (ppmw-hr) experienced by a gas turbine is matched by increasing the particulate concentration (ppmw) and decreasing the operational time to a length that was manageable in a laboratory environment. This thesis describes an experimental investigation using accelerated deposition that examined the evolution of deposits and their effects on film-cooling.

Chapter 2 documents previous work performed on the effects of deposition on film cooling. The first section highlights several studies in the literature that examined the mechanisms of deposition. The second section examines the literature for facilities that have

been developed over the years to perform accelerated deposition studies. The third section will detail the relevant factors that contribute to the formation of deposits. The fourth section will discuss the effects on heat transfer that surface roughness can cause. A wrap up of the literature review that highlights the uniqueness of the current study is at the end of Chapter 2.

Chapter 3 details the facility setup and modifications to the high-pressure aerothermal test facility located at the Department of Energy's (DoE) National Energy Technology Laboratory (NETL), in Morgantown, WV. The facility was upgraded with a high pressure particle seeder, redesigned injection port to seed fly ash into the test section, and test articles to simulate the pressure side of first stage vane. A discussion of the process used to manufacture the fly ash will also be described.

Chapter 4 details the initial testing to check the operation of the facility or "shakedown testing". Several results showed that there were some issues that needed to be addressed before the final test plan was executed. A detailed explanation of several analyses is included in this chapter. A Stokes analysis was performed to determine the particle size scaling in relation to the particles as they approached the coolant jets exiting the film cooling holes. A lumped mass analysis was performed to determine that the coal fly ash particles were at thermal equilibrium to ensure that the particles were molten before they impacted the test article. Finally, a rudimentary analysis was performed to analyze whether the injection of the particulate matter was penetrating far enough into the flow.

Chapter 5 describes the main testing phase and corresponding results. A description of the final test plan and what variables were examined are explained. The results of each different case are presented in this section. A brief discussion of issues that followed the final testing phase will be explained in the last subsection. Chapter 6 will discuss the conclusions that were

found during the execution of this study. The author will explain issues and possible errors that were encountered during the project. Finally, some suggestions for future work and improvements to the current lab setup are discussed.

CHAPTER 2:
Review of Relevant Literature

2.1 Deposition Mechanisms and Issues

The need to understand the development of particulate deposition is important to increase the life of the hot stage components in an integrated gasification combined cycle (IGCC) gas turbine. Deposition can have a devastating effect to the film-cooling scheme by altering cooling patterns both upstream and downstream of the cooling holes. Deposits in the turbine section form as ash that travels through the combustor becomes molten and starts to adhere to the first stage turbine vanes [4]. An image of the path of deposition was created by Logan et al. [4] and shown below in Figure 2.1.

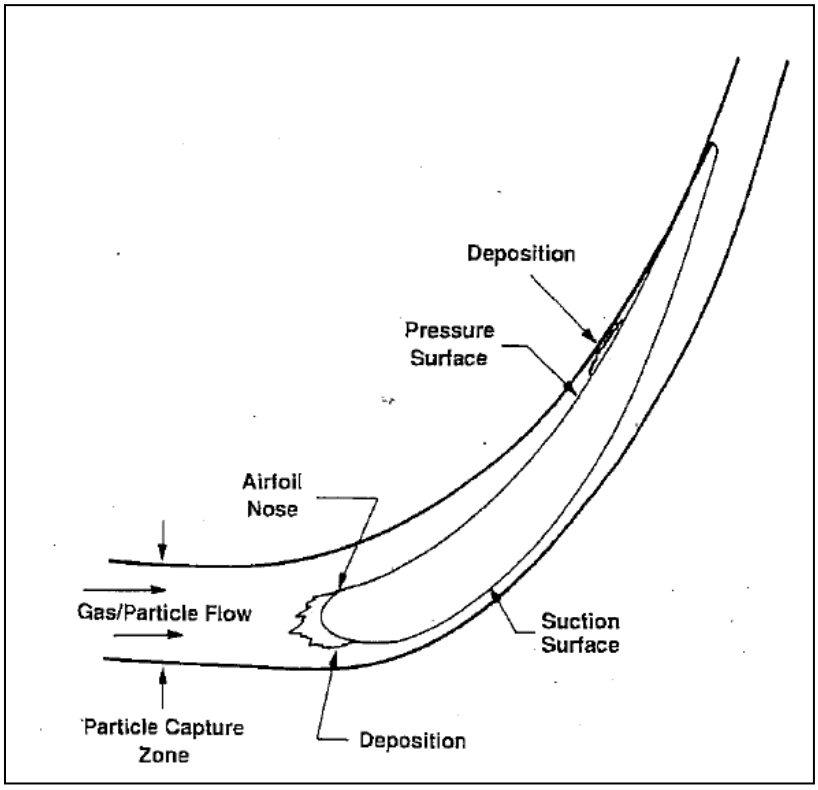

Figure 2.1. Particle deposition capture zone on a gas turbine vane [4]**.**

Bogard and Thole [7] discussed the causes of roughness being deposition, spallation, and erosion. The rougher surfaces could potentially lead to early boundary-layer transition, thickening of the boundary layer, and an increase in the turbulent mixing in the boundary layer. They reported that generally the roughness will lead to reduced film cooling effectiveness. In recent years, more emphasis has been placed on understanding the evolution of particulate deposition, its effects on thermal barrier coatings (TBC) and the effects it has on heat transfer and film cooling.

An understanding of the mechanisms of deposition is important to accurately simulate deposits in a combusting flow. Hamed et al. [3] listed the four mechanisms of particle deposition as inertial impaction, turbulent diffusion/eddy impaction, Brownian diffusion and thermophoresis. Richards et al. [8] described three effects of the deposition process being particle adhesion, deposit erosions and deposit spallation. The facility used in the study by Richards et al.[8] was a high-temperature facility at 1 atm pressure with fly ash injection. The flow would impinge on a backside cooled flat coupon where the fly ash would be deposited. They concluded that as the surface temperature of the test article increased, the ability of the particulate matter to "stick" to the surface increased.

Understanding roughness characteristics is important to the process of modeling accurate surface roughness by accelerated deposition. Bons et al. [9] examined almost 100 land-based turbine components and analyzed them to create 3D surface maps of the surface roughness. This work showed the evolution of degradation in the blades from pitting, to craters and finally exposed metal. The deposits near film cooling holes were found to increase at the point where cooling air was injected and also downstream of the holes. An important conclusion was that there was no region on a modern gas turbine blade that could not be covered by deposition;

however, the leading edge and pressure surface displayed more deposition than the suction surface. Measurements of roughness were reported for several different statistical representations of roughness, reporting values for centerline averaged roughness (R_a), RMS roughness (R_q) and maximum peak-to-valley roughness (R_t), as well as other statistics. For the purpose of the current study, the RMS roughness (R_q) and centerline average roughness (R_a) were chosen as the statistical parameters of interest for surface roughness. The centerline averaged roughness and RMS roughness are defined in Equations 2.1 and 2.2, respectively as:

$$SR_a = R_a = \frac{1}{N}\sum_{i=1}^{N}|y_i| \tag{2.1}$$

$$SR_q = R_q = \sqrt{\frac{1}{N}\sum_{i=1}^{N}y_i^2} \tag{2.2}$$

where y_i is the surface height measurement at each location, compared to the mean surface height and N is the number of measurements over the test surface. The study by Bons et al. [9] reported RMS roughness (R_q) data ranging from 1.3 μm for clean hardware to 52.5 μm for heavily serviced hardware with TBC coating spallation.

2.2 Accelerated Deposition Studies and Facilities

In order to study the mechanisms and effects of deposition on film cooling, aerodynamics and heat transfer several groups developed experimental facilities. These groups developed facilities to accelerate deposition to understand the growth and effects of deposition that occurs over the course of thousands of operating hours in a manageable time frame that could be completed in a laboratory setting. Accelerated deposition simulations match particulate loading (ppmw-hr) by increasing the particulate concentration (ppmw) for a shorter duration test. A few of these facilities were Jensen et al. [10] Turbine Accelerated Deposition Facility (TADF)

located at Brigham Young University (BYU), Smith et al. [11] Turbine Reacting Flow Rig (TuRFR) at The Ohio State University (OSU), and Lawson and Thole's [12] low speed wind tunnel at The Pennsylvania State University (PSU). At BYU Jensen et al. [10] developed the TADF to simulate 10,000 operating hours in a 4-hour test by depositing material onto a flat coupon. The facility matched the Mach number and flow temperature of the first stage high-pressure turbine vanes but did not match the pressure. Jensen et al. concluded that the surface topography, microstructure and chemical composition found in the accelerated deposition process resembled actual industrial gas turbine deposition therefore the process was adequate to simulate deposition.

Smith et al. [11] developed the TuRFR to simulate deposition on nozzle guide vanes in combusting flow during a 1-2 hour test. Coal ash was injected into the flow at high particulate loadings to simulate the particulate deposition of several thousand hours of run time. The test article consisted of two nozzle guide vane (NGV) doublets. The TuRFR facility was capable of matching the temperature and inlet Mach number of an industrial gas turbine but not at elevated pressures. The conclusions from this work showed that this method of accelerated deposition was sufficient for simulating roughness characteristics caused by deposition on actual engine hardware. The pressure surface and leading edge showed significantly more deposition than the suction surface. The study concluded that film cooling reduced the evolution of surface deposits which was consistent with the study by Bons et al. [9] that described furrows developing downstream of the cooling holes.

Lawson and Thole [12] used a low-speed wind tunnel with low melting temperature wax to simulate particle deposition. Non-dimensional Stokes similarity was used to scale the inertial characteristics of fly ash particles in engine conditions by using larger wax particles in laboratory

conditions. A large-scale open loop test channel was used to examine the effects of deposition on a film cooled flat plate at conditions close to standard temperature and pressure. Albert and Bogard [13] performed experiments in a facility similar to one used by Lawson and Thole. The main difference was that the wax was being deposited onto a large scale 2-passage vane cascade.

2.3 Relevant Variables in Deposition

It is important to understand how independent variables (impaction angle, freestream temperature, etc.) affect the evolution of deposits. As discussed earlier, the TADF, developed at BYU, has been employed to perform numerous studies of the factors affecting deposition ([6],[10], [14], [15], [16], [17], [18], and [19]). Bons et al. [6] performed a study examining the deposition from four different materials: straw, sawdust, coal and petroleum coke (petcoke). The four different materials were being studied to determine which material would simulate deposition adequately. The results showed that more deposition formed from coal and petcoke than straw and sawdust. The main finding related to this study was that the coal and petcoke deposit structures were found to detach easily from the turbine material with thermal cycling and handling. Jensen et al. [10] looked at the influence of the impaction angle on the deposit formation. Tests were performed at impaction angles of 30^o, 45^o and 90^o with the same inlet jet Mach number and temperature. The 30^o and 45^o angles represent impaction angles on the pressure side of a turbine vane while the 90^o angle was representative of the leading edge of a turbine vane. The results showed that as the angle increased to an impingement of 90^o the amount of deposition on the coupon increased. Crosby et al. [14] experimented on the effects of particle size, gas temperature and metal temperature on ash deposits using two different types of turbine syngas. Four series of tests were performed in the TADF to test the effects of each one

independently. In the first series, four different particle diameters ranging from 3-16μm were used to examine the effects of the different particle sizes on deposition. Larger particles would cool down faster as they approached the film-cooled surface than smaller particles. The inertial characteristics of the larger particles preclude them to be more likely to continue on their initial trajectory as the flowpath moves around the component. Figure 2.2 displays an image of the trajectory of large and small particles as the the flow path turns and interacts with the boundary layer.

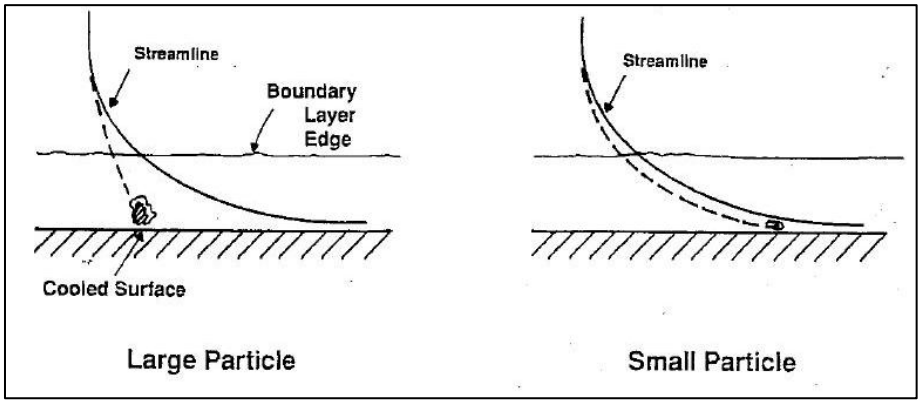

Figure 2.2. Comparison of larger particles and smaller particles reactions to change in flowpath [4]**.**

The capture efficiency (ratio of mg/hr of deposit divided by mg/hr of particulate matter added to flow) more than doubled as the particle diameter increased from 3 to 16 μm. When the gas temperature was reduced the rate of deposition decreased. At temperatures below 960 ^{o}C no deposition was observed. Ai et al. [15] used the TADF to perform experiments on cylindrical holes, with and without TBC coating, with film cooling blowing ratios ranging from M=0.5 to 4.0. The equation for the blowing ratio, M, in this study is shown below in Equation 2.3.

$$M = \frac{\rho_c U_c}{\rho_\infty U_\infty} \tag{2.3}$$

The “bare” coupons (i.e. without TBC) had approximately an order of magnitude fewer deposits (in terms of weight) than their TBC counterparts. Several experiments were performed to examine the effect of the blowing ratio. At the lowest ratio of 0.5 the deposition occurred around the cooling holes. The holes became partially blocked and resulted in higher surface temperatures. At M=2.0 the deposition that occurred downstream of the holes had “ridges” between the holes and less deposition in the coolant path. The general conclusion with regards to the effect of blowing ratios was that as blowing ratio increased the surface temperature began to decrease and the coolant coverage began to increase. As discussed above, the surface temperature is a crucial component of deposition so anything that lowers the surface temperature over a larger area would result in less deposition. Another result was that as the duration of exposure increased the amount of deposition on the face of the coupon increased. Ai et al. [16] performed a study looking at the effects of hole spacing and surface coating on deposition. The results of this study showed that the deposit structures were more likely to flake off of the bare metal coupons during the cool down phase than the TBC coated test articles at the same hole spacing setup. The capture efficiency was higher for the TBC coated coupons than the bare metal coupons for the same hole spacing setup also. The dominant factor for deposition appeared to be surface temperature based on the results.

Wammack et al. [17] performed a study using the TADF to examine the evolution of deposits by performing 4 successive 2-hour deposition tests. By increasing the particulate concentration from the typical gas turbine concentration of 0.02 ppmw (parts-per-million-weight) to 20 ppmw the tests would simulate 10000 operating hours in 10 laboratory hours. The total laboratory test time was split into 4 different parts to examine the deposition build up of 3

months of simulated operating time. Three different test coupons were used: bare polished metal, polished thermal barrier coating with bondcoat and unpolished oxidation resistant bondcoat. Despite the three different surfaces, the deposition for all three was similar after repeated exposure. The bare metal coupons took longer for the deposit structures to begin to form. The interval testing showed that an initial deposition would occur that had peaks and valleys. Then another layer would come and fill in the valleys. Then with successive tests, another layer would form and fill in the valleys from the previous tests. Ai et al. [18] performed experiments on the effects of particle size on the deposition. Two different sizes of coal ash were used in this experiment with mass mean diameters of 4 and 13 micron, respectively. The tests were conducted in one hour intervals with a particulate concentration of 160 ppmw. The results showed that larger particles created more deposition than smaller particles. The smaller/finer particles were shown to be much harder to remove once the test was over than the larger ones.

Laylock and Fletcher [19] performed experiments in the TADF studying the amount of deposition over different periods of time. The TADF was set at inlet Mach number of 0.25 and an inlet temperature of 1250^{o}C. Tests were performed at 20, 40, and 60-minute intervals. The results showed that the capture efficiency (measure of the amount of deposition on the coupon divided by the difference of the injected amount minus the amount found in the inlet tube) increased as the amount of time increased. This proved that as deposition formed on the surface of a component it becomes more suitable for further deposition to form.

Webb et al. [20] used the TuRFR to examine the effects of different compositions of fly ash would have on the ability of the fly ash to deposit onto the components. The mean diameter of the particles was approximately 10-20 μm. The study performed tests at different inlet

temperatures ranging from 900-1200^{o}C. They found that the mainstream temperature needed to reach between 1044-1060 ^{o}C depending on the composition of the fly ash to soften the particles enough to cause deposition. Film cooling was used on a limited amount of cases and proved to be ineffective in cases of severe deposition.

Lawson and Thole [12] found that deposition decreased with an increase in coolant mass flow because coolant jets diverted particle trajectories and cooled particles preventing them from sticking upon impacting the surface. Albert and Bogard [13] examined an isothermal vane and an internally cooled vane. The results showed that the surface temperature plays an important role in deposition. The isothermal blade had significant deposition along the pressure side while the internally cooled blade had very little deposition in the same area.

2.4 Relevant Surface Roughness Heat Transfer Effects

The current study does not include surface temperature measurements to determine heat transfer coefficients or cooling effectiveness, however this work is planned for the future testing and a review of some relevant studies is included herein. The following studies show the effects of the surface roughness created by deposition on gas turbine heat transfer. Using the TADF, Bons et al. [19] performed research on how the heat transfer was affected as the deposition evolved. Their work produced a couple of important conclusions. The heat transfer coefficient (St) had a "comparable plateau" that matched the pause in deposition growth discovered by Wammack et al. [15]. The largest jump in St occurred between burns 1 and 2. The cause of this was due to "peaks" that were created as the deposition began to accumulate on the blades. The St leveled off between burns 2 and 3 as the deposition began to fill in the valleys between the

peaks. They credited this to the deposition having an "insulating" effect on the turbine blade. Between burns 3 and 4 there was another increase in St as more peaks were formed.

Erickson et al. [21] performed experiments on the vane heat transfer, with simulated surface roughness, while incorporating the influence of the turbulence conditions and Reynolds number. Their experiment tested both a smooth and realistically rough surface vane. It was concluded the realistic roughness seems to not have any influence on the Stanton number as long as the boundary layer remained laminar. Another conclusion was that realistic roughness led to an early transition from laminar to turbulent. This was the same regardless of the turbulence condition that was tested. This conclusion was consistent with previous studies.

Lewis et al. [22] performed experiments on the film cooling effectiveness and heat transfer near cooling holes. Deposits were accumulated on three different turbine coupon setups with film cooling. One setup had a large deposition pattern that was only upstream of the holes, the second had a large deposition pattern extending downstream of the cooling holes and a third had a small deposition pattern that extended down between the cooling holes. Scaled plastic models of the deposition were inserted into a low-speed wind tunnel. The models were then used to measure film cooling effectiveness and heat transfer coefficients. In areas where the roughness was located upstream of the film holes, it was concluded that the area averaged heat flux is lower on the coupon with deposition than without. The authors state that the reason for this is the "effective ramp" that is created by the deposition and creates a space for the film cooling to reside. For the roughness patterns that extended down between the holes a smooth area was created that allowed the coolant to travel. In the smooth area the heat transfer levels are much lower and the effectiveness levels are much higher. The "furrows" that form downstream

of the holes between the cooling jets are experimentally important because the same “furrows” have been found on actual hardware parts.

Based on the work reported above it is clear that deposition has a detrimental effect on gas turbine film cooling. Understanding the evolution of deposition and its effects on heat transfer and cooling of turbine components in realistic engine conditions is critical to reducing the downtime of industrial gas turbines. The previous work in this field has produced significant results on the effects of gas temperature, particle sizing and surface temperature as well as other factors that influence the evolution and growth of deposition at low temperature and elevated (more representative of turbine operating conditions) temperatures. However, none of these studies have simulated the high pressures that exist in an actual gas turbine. The current study describes the methods developed to simulate accelerated deposition to produce roughness characteristics representative of a gas turbine engine at elevated pressures and temperatures to examine factors that increase particulate deposition by modifying an existing high-pressure combustion facility.

CHAPTER 3:
Experimental Facility

3.1 High-Pressure/Temperature Combustion Facility

The project was conducted in the National Energy Technology Laboratory (NETL) High-Pressure Aerothermal Test Facility located in Morgantown, WV. The test facility, shown below in Figure 3.1, was originally designed to perform combustion testing, but in recent years has been converted over to a turbine-related aerothermal and heat transfer research facility. The current study was performed at a hot gas path pressure of 4 atm. Six independently controlled flow loops were used to supply pressurized air for combustion and cooling at a maximum combined flow rate of 0.9 kg/sec. The fuel supplied to the facility was natural gas and entered the combustion area through two independent flow loops that had a maximum combined flow rate of 12 g/sec and a mainstream test section velocity of 64 m/s.

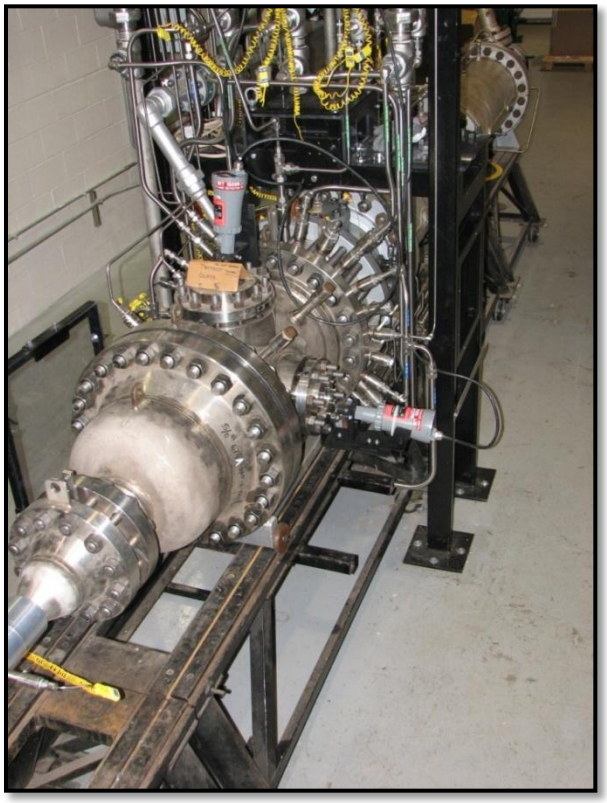

Figure 3.1. NETL High Pressure Aerothermal Facility.

The combustor section located upstream of the aerothermal test section was designed as a swirl-stabilized, lean premixed combustor that provides swirling, turbulent, high temperature flow to the test section region. The combustion region was bounded by a fused silica tube liner with a 180 mm inner diameter and 300 mm length. This liner allowed for optical access on three sides of the test facility. Directly downstream of the combustor region the diameter was reduced to 105 mm to enter the water-cooled walls of the combustor exhaust duct. The water used to cool the combustion exhaust duct was not mixed with the hot process gas and no film cooling was used upstream of the aerothermal test section.

Directly downstream of the combustor exhaust duct was the transition piece that converted the dimensions and shapes of the flow path from a circular cross section to a rectangular cross section. The rectangular cross section's dimensions were 51 mm wide by 127 mm high. High-density zirconia refractory was used to cast the transition piece while the rectangular walls of the test section were constructed of a conventional high-alumina, dense-castable refractory. An insulating refractory layer was used to house the test section and protect the pressure vessel walls from the hot gas path.

Carbon steel components were used to construct the pressure vessel for this test section. Three 10 cm diameter ports were oriented 90^{o} apart around the circumference of the 46 cm diameter carbon steel vessel. One of the ports was used to install the test article while the port 180^{o} around the pressure vessel was used to house the optical quartz windows. The port that was oriented 90^{o} between the other two ports was used to monitor the hot gas temperature using three conventional (Type-K) thermocouples. One thermocouple protruded into the flow 2.54 cm, the second was positioned to be flush against the refractory wall, and the last thermocouple was

positioned approximately 2.54 cm into the refractory. An image of the cross-section of the high-pressure combustor and test section is shown in Figure 3.2

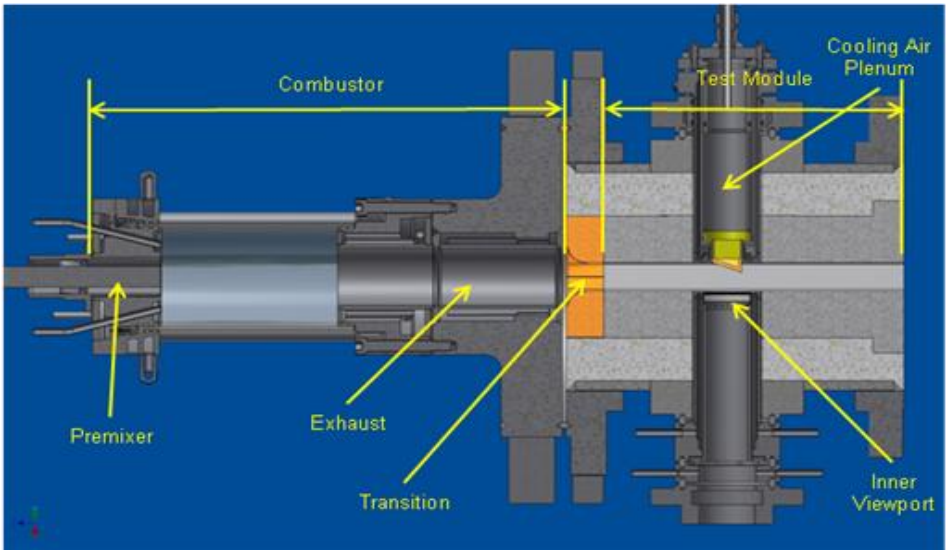

Figure 3.2: Cross sectional view of the combustor, transition piece, and aerothermal test section.

Haynes 230 material, provided free of cost by Haynes International, was used to construct all test articles used for this study (described in section 3.2). The test articles were mechanically compressed into place when they were installed into the holder. The holder was positioned to create a flush plane with the hot gas path. A ceramic gasket material was positioned between the test article and the holder to attempt to reduce conduction losses. The test article holder is shown below in Figure 3.3.

Figure 3.3: Image of test article holder.

Cooling air was supplied through a 12.7 mm diameter tube to the cooling air plenum. The cooling air was at room temperature as it entered the plenum for this study. The plenum was approximately 326 mm long with a diameter of 67 mm from the cooling air entry point to the back of the test articles. The cooling air was injected as film cooling air into the main flow through four cooling holes. All cooling air in the plenum was injected through the cooling holes. Approximately 25 mm away from the test article a thermocouple (Type-K) was positioned to measure the cooling air temperature. The estimated bias uncertainty for this thermocouple reading was approximately 5-10K.

A single-wavelength infrared (IR) imaging technique was used to measure the surface temperature on the hot-gas side of the test article. This method was used because it was not intrusive and did not require contact with the surface. Several disadvantages were associated with this method and will be discussed in more detail in a later chapter. The reflections from the surrounding hot walls introduced a significant uncertainty into the measurements. Another

uncertainty involved the variations of the emissivity, or reflectivity, of the surface of the test article that were caused by surface oxidation at high temperatures. The inner quartz sight glass devitrified (changed phase) during the testing time and this effect altered the transmissivity of the window. Solutions for these uncertainties were not completed at the time of this thesis but a description of the process is included to demonstrate the initial method development.

The viewport assembly, shown below in Figure 3.4, was located directly across the channel from the test article. Two quartz windows were mounted in the optical viewport assembly. The interior window had dimensions of 76.2 mm diameter by 12.7 mm thick and was situated flush with the interior test section wall. The window started to devitrify at temperatures above 1000^{o}C. This devitrification results in significant optical transmission loss. The outer window was a commercial sight glass that was mounted outside of the pressure vessel and was used as the outer pressure boundary. Figures 3.5 and 3.6 display an isometric view of the test section and a cross section view of the flow path through the test section[23].

Figure 3.4. Image of viewport assembly.

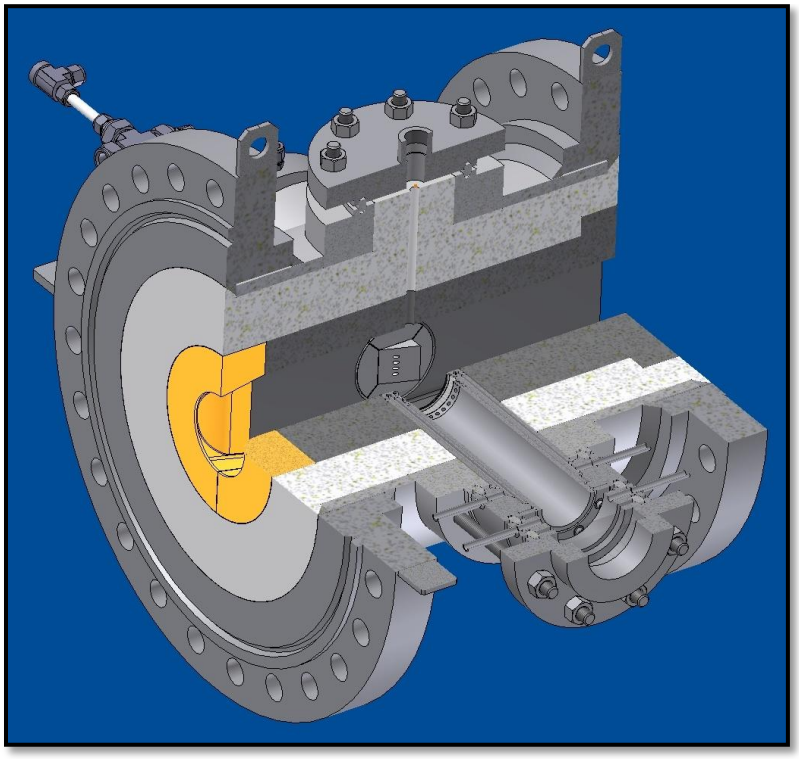

Figure 3.5. Isometric view of the aerothermal test section.

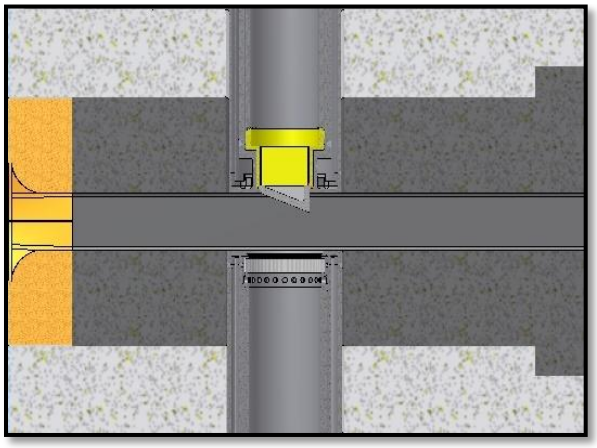

Figure 3.6. Cross section of the flow view.

3.2 Test Article Design

Test articles were designed to simulate the pressure side of a first stage turbine vane at 10^o and 20^o angles. As explained in section 2.2 the leading edge and pressure surfaces are where the majority of deposition occurs. Figure 3.7 displays two views of both the 10^o and 20^o test articles. The two angles of the test articles were selected to simulate the pressure side of a first stage vane since the facility could not incorporate actual blade geometries. There are many impaction angles on an actual turbine vane, ranging from 90^o at the leading edge to 0^o downstream of the leading edge on both the pressure surface and suction surface as seen in Figure 2.1, where the red lines denote the hot gas flow path. Angles of 10^o and 20^o were selected to represent an obstruction without impinging into the flow too much.

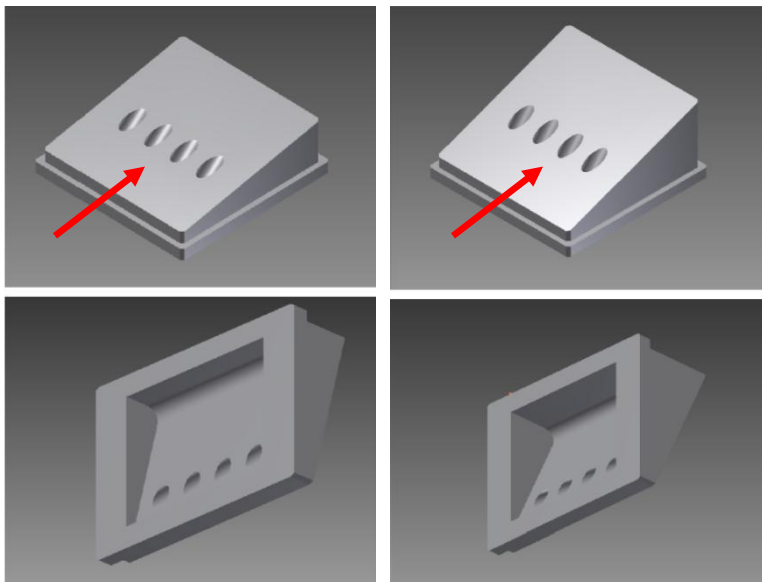

(a) **(b)**

Figure 3.7. 3D model of front side and back side of the (a) 10^o test article and (b) 20^o test article.

The backside of both of the test articles was hollowed out to supply backside cooling evenly to the face. Four cylindrical cooling holes with 4 mm diameters were located on the front side of the face. The cooling holes were positioned at a 30^o angle to the face. The cooling holes

were sized by Reynolds similarity using a value provided by GE Energy based on the freestream velocity and cooling hole diameter of one of their industrial gas turbine models[24]. The cooling hole diameter was used as the length scale to simulate the obstruction that occurs as the flow encounters coolant jets on the pressure side. For the study it was important to simulate the interaction of the flow structures that occur as the mainstream flow near the wall of the pressure surface encounters the coolant jet. Equation 3.1 displays the Reynolds number equation with the cooling hole diameter and freestream values of density, viscosity and velocity.

$$Re_c = \frac{\rho_\infty U_\infty d_c}{\mu_\infty} \tag{3.1}$$

Thermal Barrier Coating (TBC) was applied to the test articles using a directed vapor deposition (DVD) process developed and applied by Directed Vapor Technologies International, Inc. (DVTI). The DVD process, shown in Figure 3.8, uses an inert gas to direct the coating medium to the surface of the test article. The bond coat was the γ–γ' Platinum Aluminide developed by Dr. Brian Gleeson at the University of Pittsburgh. The TBC was 7% Yttrium Stabilized Zirconia (7YSZ), an industry standard in TBC coatings. Table 3.1 displays the layers and their corresponding thicknesses. A cross sectional view illustrating a TBC coating system on a turbine blade is displayed in Figure 3.9. The base metal is first coated with the bond coat followed by the TBC layer.

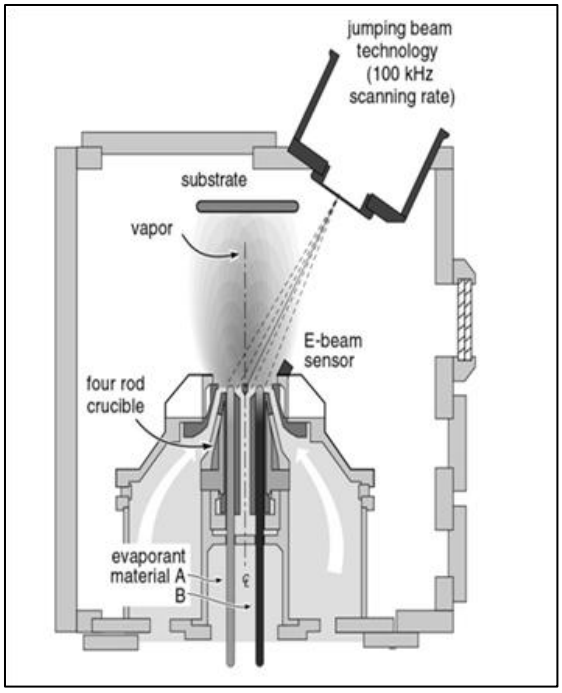

Figure 3.8. Schematic of the directed vapor deposition process developed by Directed Vapor Technologies International, Inc [25].

Table 3.1. Coating Layer Details [25].

Layer	Type	Thickness
Bond Coat	γ-γ' PtAl (Dr. Brian Gleeson, UPitt)	~15-20mm
Thermal Barrier Coating (TBC)	7% Yttrium Stabilized Zirconia (7YSZ)	~200-500mm

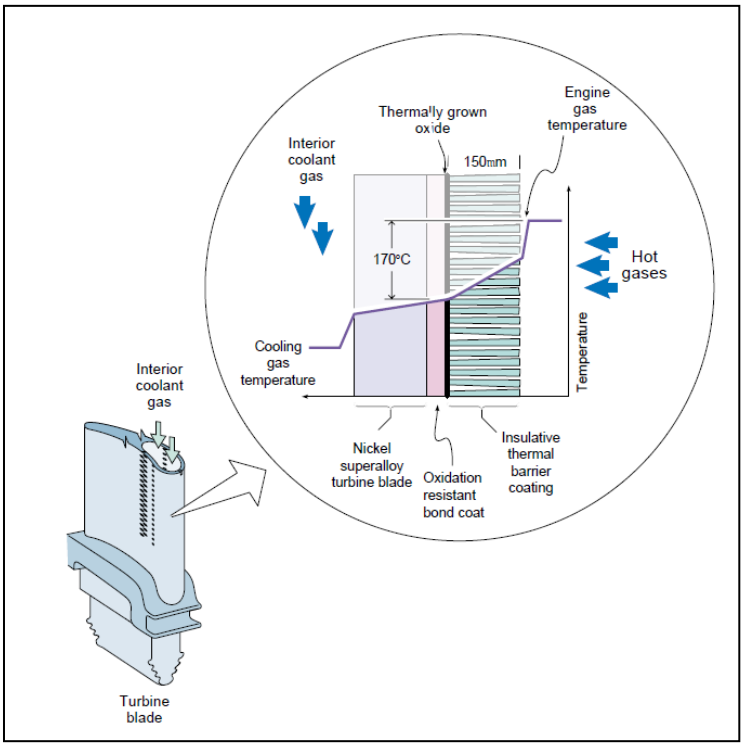

Figure 3.9. Cross sectional view of the blade metal through TBC layer [25].

3.3 Scitek PS-20 Particle Seeder

In order to perform accelerated deposition testing, a system to seed the mainstream flow with particulate was developed by procuring a Scitek PS-20 particle seeder which is shown below in Figure 3.10. The particle seeder was designed to be pressurized up to 20 atm to create enough back pressure to seed into high pressure environments and is generally used in experimental fluid mechanics facilities as a Particle Image Velocimetry (PIV) particle seeder [26]. High-pressured Nitrogen was used as the gas that entrained particles from the seeder and injected them into the test section. It is important to note that Nitrogen was selected as the gas because it was an existing open flow loop available in the facility and did not serve any other purpose. This gas entered the pressure vessel by traveling through 5 separate nozzles. The

nozzles exited on the bottom of the pressure vessel where the fly ash was deposited from a particulate canister shown in Figure 3.11.

Figure 3.10: Image of Scitek PS-20 Particle Seeder [26].

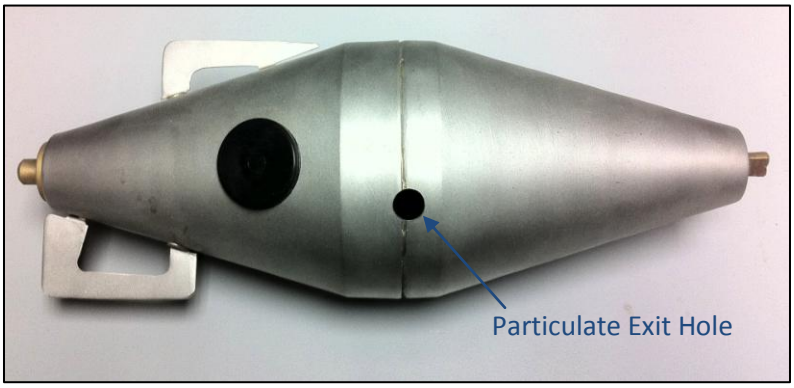

Figure 3.11: Image of particulate canister.

The motor in the particle seeder was variable controlled with a 12-volt potentiometer. In order to set the rate of injection of fly ash into the combustion facility, several iterations were performed of setting the input voltage to the seeder, running a test for set durations and measuring the difference of weight of fly ash in the canister. The rotation of the particulate canister deposited material into the main chamber so it could become entrained in the flow and

exit the main chamber. Two fins were attached to the canister to break up agglomerated material. The particulate matter exited through stainless steel tubing and entered the water cooled injection tube. A cross section view is provided in Figure 3.12 to explain the process.

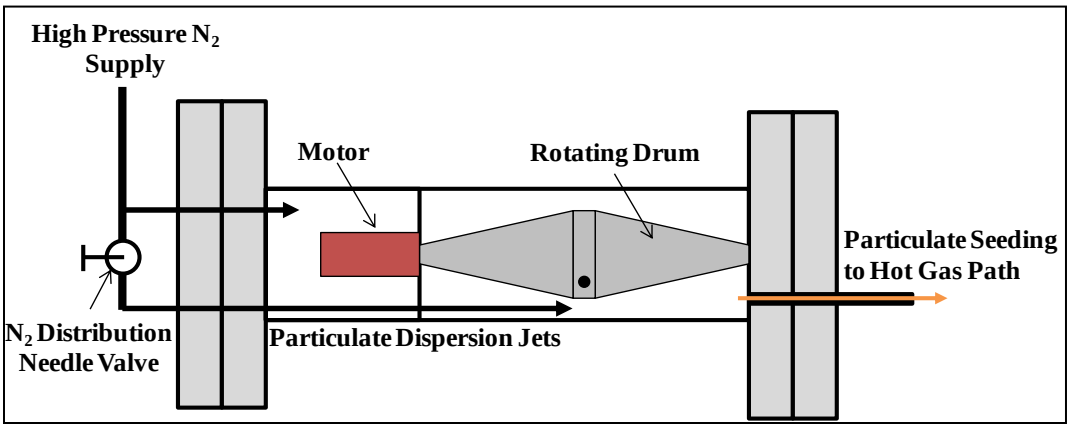

Figure 3.12: Cross sectional view of particle seeder setup.

3.4 Injection Tube Redesign and Port Locations

Modification of the high-pressure facility to seed fly ash into the test section was accomplished by modifying an existing water-cooled port. The port was water cooled to prevent compromising the metal due to temperature increases from contact with the hot gas path. A redesign of the port was required to allow seeding into the high pressure environment. In the original design the cooling water entered through the top of the port. For the redesign this cooling water entrance was moved to the side of the tube and a ¼ inch tube was placed down the center and opened into the test section just upstream of the transition piece. An isometric view of the redesigned tube is shown in Figure 3.13, shown below.

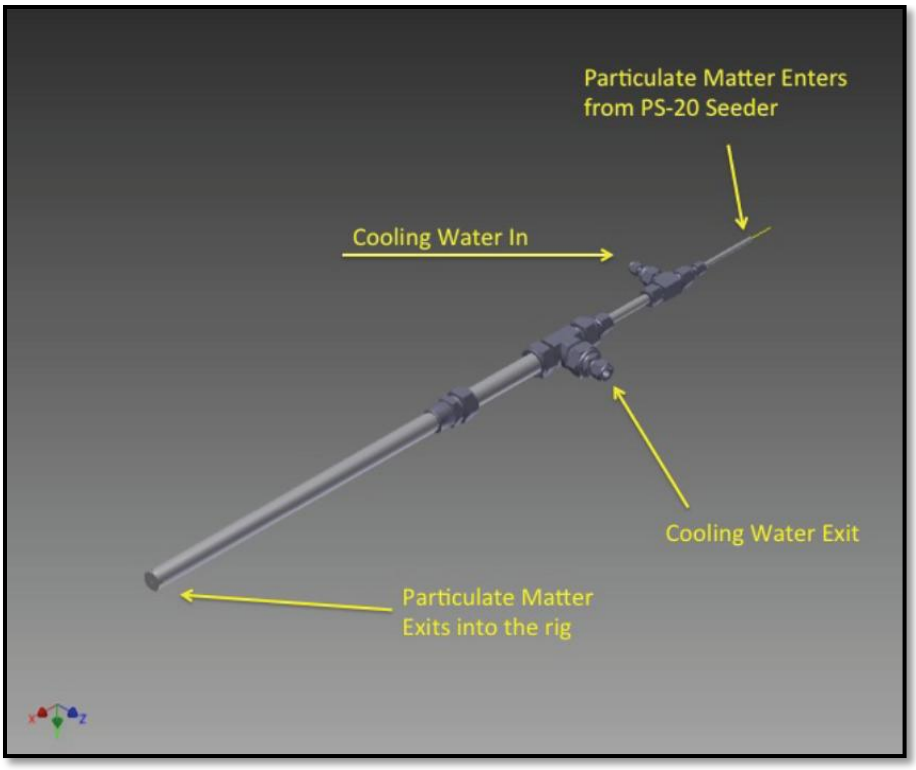

Figure 3.13. Isometric view of the water cooled injection tube.

The injection tube port was located between the combustor and the aerothermal test section, as shown in Figure 3.14. The location was approximately 14 inches upstream of the test section. A port map is shown in Figure 3.15 to show the ports attached to the aerothermal test section. Every test performed in the high-pressure facility requires ports for cooling air and water to keep the facility temperature below a set temperature that would compromise the integrity of the external shell. Several unused ports were installed to allow flexibility of the test section to be used for numerous different types of experiments such as the current study.

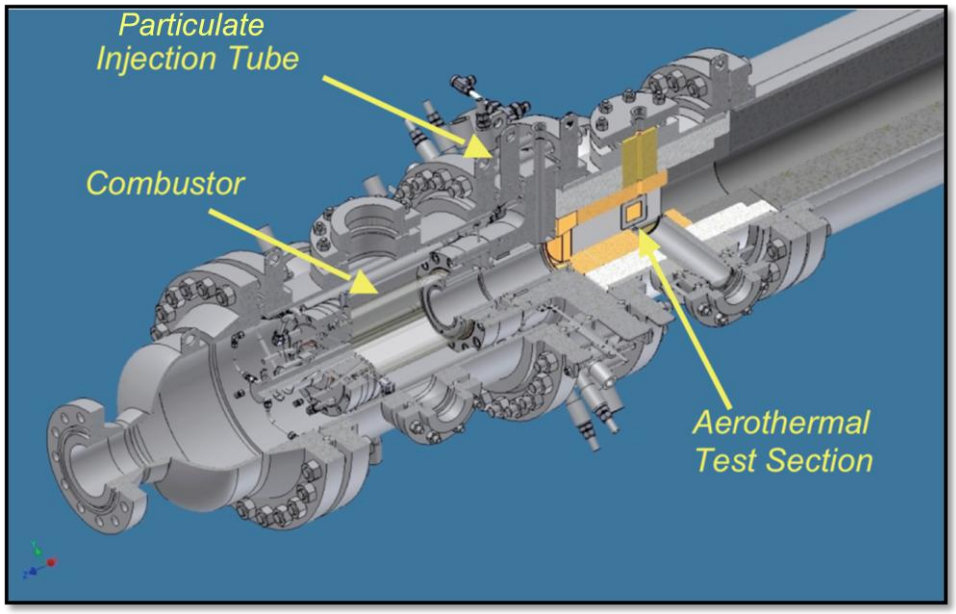

Figure 3.14. Isometric view of the aerothermal test section, injection port and combustor.

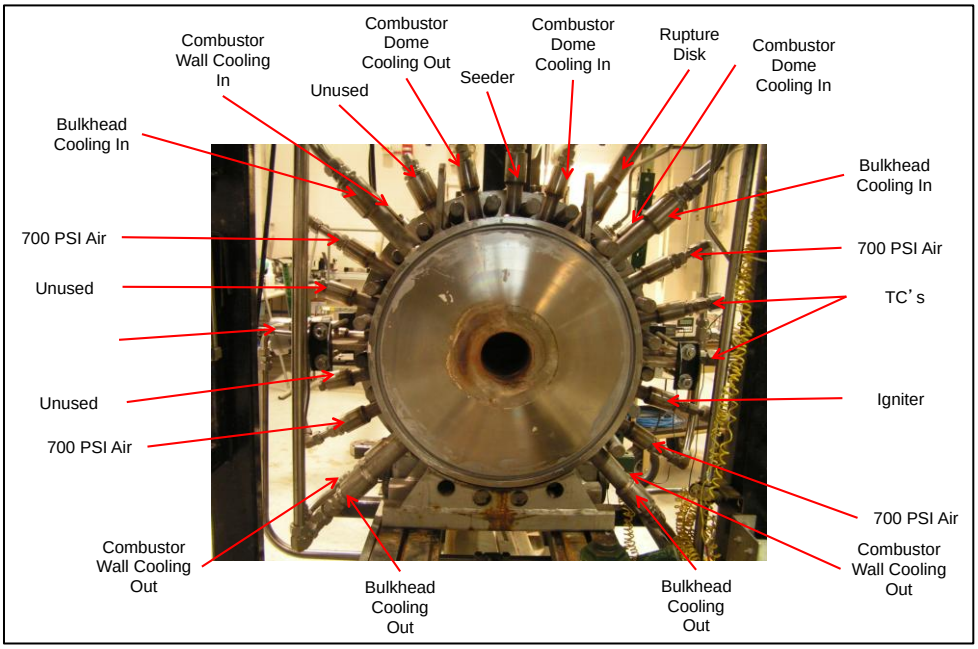

Figure 3.15. Port map for the aerothermal section.

3.5 Fly ash Sizing and Processing

To model the deposition in IGCC turbines it is not reasonable to run tests on a 1:1 basis with the operation time of an actual turbine being measured in thousands of hours. An accelerated deposition process, similar to studies performed in the TADF and TuRFR, was developed to simulate 10000 operating hours in a manageable time frame to perform experiments. The particulate concentration in an industrial gas turbine is estimated from operational data to be 0.02 parts-per-million by weight (ppmw) based on the literature [27]. For this operational timeframe and concentration, this yields a particulate loading of 200 ppmw-hr. A particulate concentration that matched the particulate loading of the engine was calculated to be 33.33 ppmw with an operation time of 6 hours. Table 3.2 displays the values of the accelerated deposition calculations.

Table 3.2. Accelerated Deposition Parameters.

	Engine	Laboratory
Particulate Concentration (ppmw)	0.02	33.33
Operation Time (hr)	10000	6
Particulate Loading (ppmw-hr)	200	200

In addition to particulate loading, modeling the size and composition of the particulate in the hot gas path was critical to producing accurate deposition. The mean particle diameter of particulate matter in a gas turbine is estimated to be less than 10 μm when the filtration system is working correctly as mentioned in chapter 2. As filtration systems begin to wear larger particles of varying unknown sizes may travel through the engine. A method was developed to process the flyash to be injected into the high-pressure combustion facility. The flyash was baked for approximately 45 minutes in a toaster oven to remove all moisture. A flourmill was used to

grind the flyash. Particles larger than 45 microns were filtered out using a shake table. The composition and sizing analysis of the particulate matter was performed by Intertek in Chicago, Il. The mean particle size was approximately 13 microns [28]. Table 3.3 below displays the comparison of the bituminous flyash composition by weight between the current study and Smith et al. [11].

Table 3.3. Flyash Comparison.

Composition	Smith et al. [11]	WVU
SiO2	32.9	53.8
CaO	2.93	4.39
Fe2O3	40.6	8.87
Al2O3	20.3	25.35
SO3	0.827	1.15
K2O	2.48	2.23

Several different flyash processing methods were attempted before selecting the method described above. Figure 3.16 displays three different fly ash processes' size distributions compared to the size distribution being matched from literature. The first process, labeled WVU1, was fly ash that was baked and put through the flower grinder. Only the flyash that was caught in the grinder filter was used for WVU1. It can be seen in the figure that the size distribution was too fine to match the size distribution from the literature. This process also took significant time to get adequate material to be analyzed, and would require too much time to process a sufficient to complete testing. The second process, labeled WVU2, repeated the same procedure except that instead of using the fly ash caught in the filter the flyash that came out of the grinder was used. This size distribution was closer to the distribution in the literature but there was a significant amount of larger particles that weren't needed. This can be seen in the last peak around 60 μm of the WVU2 particle size distribution. Finally, process 3, labeled

WVU3, was selected as the final procedure to get the required level of fly ash processing. This process was exactly the same as WVU2 except that after the grinder was used the fly ash was sieved using a shake table that filtered all particles over 45 μm.

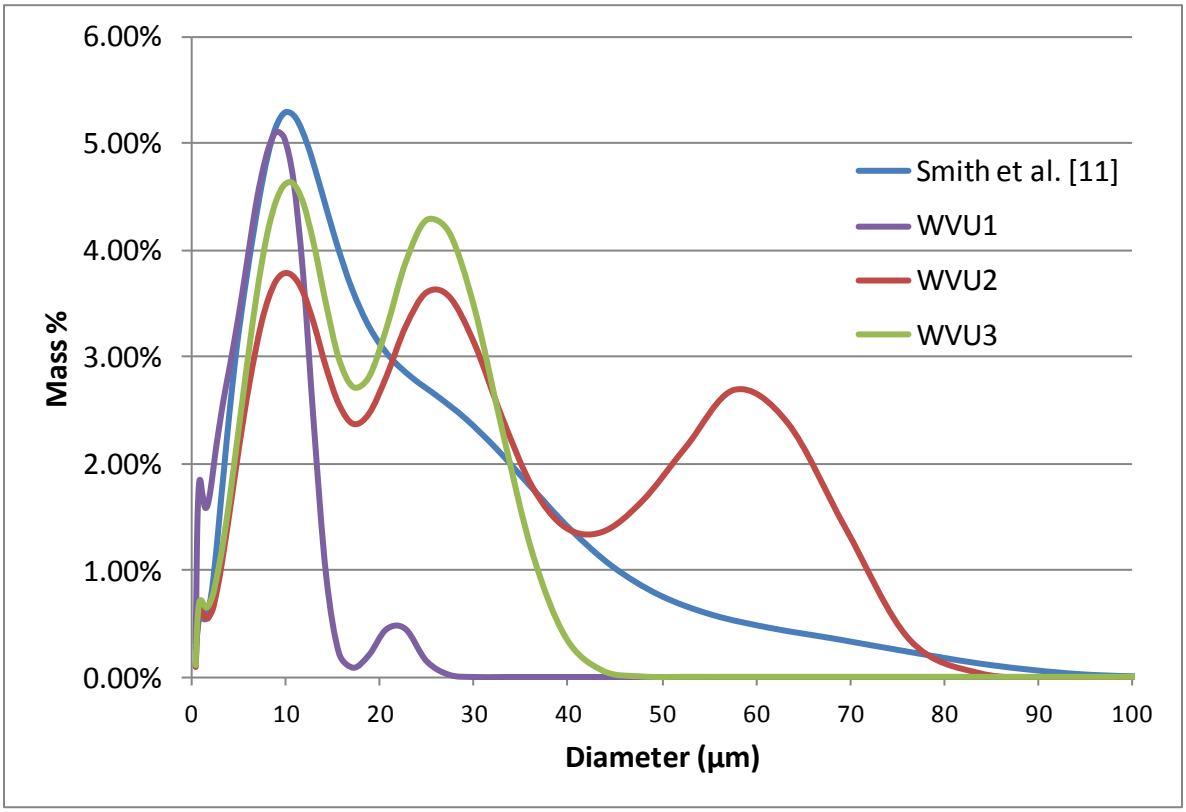

Figure 3.16. Comparison of size distributions between current study and literature.

3.6 Laser Confocal Microscope Scans

An Olympus LEXT OLS 3100 laser confocal microscope, which was provided by NETL and can be seen in Figure 3.17, was used to perform a characterization of the surface roughness of the test articles. The microscope was used with a 5 micron resolution. The computer program that accompanies the microscope was capable of filtering out noise, correcting tilts and

calculating roughness characteristics in the scanning field. The microscope was capable of scanning minute contaminations such as the silica contaminations seen in Figure 3.18. The silica deposits on the TBC were caused by a contamination during the directed vapor coating process. The contaminated test articles were not used in any of the testing performed. The laser microscope was used to take scans of the bare metal and TBC coated coupons before the tests were performed.

Figure 3.17. Olympus LEXT OLS 3100 laser confocal microscope [28].

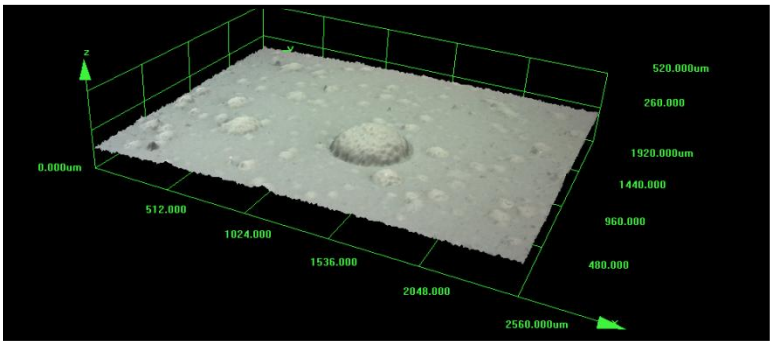

Figure 3.18. Scan of silica contamination on TBC layer at 5μm resolution.

CHAPTER 4:
Initial Facility Testing Results and Analyses

4.1 Initial Testing Results

Initial tests were performed to evaluate the operability of the test facility with the addition of the particle injection system. Initial tests were performed both with combustion and without combustion to calibrate the particle seeder to inject the correct amount of flyash into the combustion facility. The seeder was originally placed on a stand next to the aerothermal test section. During the initial testing only small amounts of fly ash were deposited into the test section due to a large pressure drop across the tubing. The seeder was moved to a position above the test section which reduced the overall length of tubing and decreased the pressure drop. The two positions of the seeder are shown in Figure 4.1.

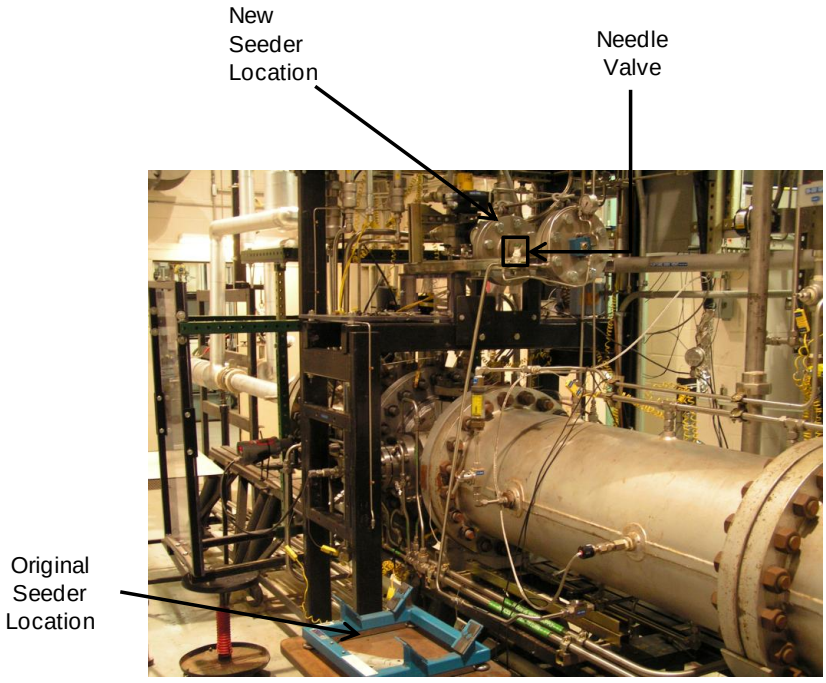

Figure 4.1. Particle seeder adjustments.

A process was developed to fill the particulate canister with an initial amount of fly ash and weigh it before insertion into the seeder. After a run the canister would be weighed again along with all fly ash still present in the pressure vessel of the seeder. The final weight would be subtracted from the initial weight to determine the amount of fly ash deposited into the test section. A layer of fly ash with a mass of approximately 50 grams was found in the pressure vessel after every run therefore an extra 50 grams was added to the initial mass. This process was performed several times during the initial testing to reach the desired particulate loading for the 3-hour test.

During an examination of the particle seeder after one of the initial runs, an issue with the jets inside the pressure vessel was discovered. The jets appeared to travel only along the bottom of the pressure vessel of the seeder. A needle valve was installed to alter the flow in the pressure vessel of the particle seeder. Pieces of Styrofoam were added to the chamber and the metered jets effectively started lifting the Styrofoam off the bottom of the chamber unlike the unmetered jets. It was theorized that this more turbulent flow would agitate more fly ash particles and increase the likelihood that they would become entrained in the flow exiting the seeder. A schematic of the final seeder setup was displayed in Figure 3.12.

Once sufficient fly ash was being injected into the test section 3-hour tests were performed on both a 10^{o} and 20^{o} test article. The conditions of these tests were at a temperature and pressure of approximately 2000^{o}F and pressure of 45 psig, respectively. Below, shown in Figures 4.2, is an image of both test articles. No visible deposit structures accumulated on either test article. The 20^{o} test article did have a red discoloration which may have been fly ash deposits. In order to examine the cause of the lack of deposit structure growth on the test article, several analyses were performed and are described in the following sections.

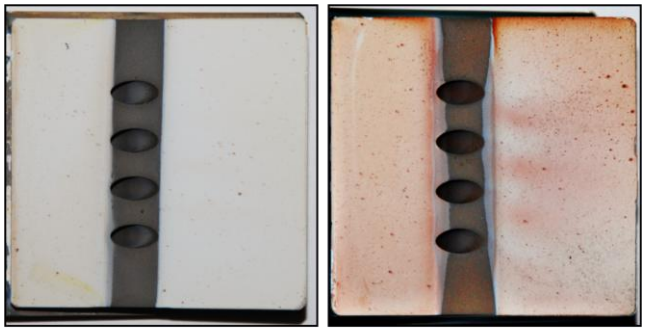

Figure 4.2. Shakedown test results of (a) 10^{o} test article and (b) 20^{o} test article.

4.2 Stokes Analysis

A Stokes analysis was performed to try and match the dynamic characteristics of the interactions between the particles in the flow and the coolant jets. Stokes number similarity was used in conjunction with Reynolds number similarity (simulating interaction of the mainstream flow with the coolant jet flow) and Blowing Ratio (to simulate ratio of coolant jet mass flux to mainstream mass flux) to try and match the particle trajectories that occur on the pressure side of an industrial gas turbine vane with the experimental test setup. It is important to note that this analysis was only simulating conditions of flow interactions near one cooling hole on the surface of the test article and not any flow structures that would occur as the jet penetrated into the mainstream flow or disruptions of secondary flow interactions from neighboring holes. The purpose of doing this similarity analysis was to match the initial flow interactions and particle inertial characteristics at the point where the mainstream flow encounters the coolant jet near the pressure surface of an industrial gas turbine vane. It is noted that the mainstream flow obstruction presented by the wedge shape of the test article used in this study was ignored. Also, this Stokes analysis ignores the presence of neighboring coolant holes. Finally, it is assumed that for a non-zero blowing ratio, there is no mixing of the mainstream and coolant flows in the

region of the test article surface and that the mainstream flow was deflected around the coolant holes only parallel to the plane of the test article surface. It is understood that for tests with no coolant flow (M=0.0) that the Stokes number as defined herein loses meaning. Equation 4.2 displays the equation for the Stokes number

$$Stk = \frac{\tau_p}{\tau_f} = \frac{\rho_p d_p^2 U_p}{18 \mu_\infty d_c} \tag{4.2}$$

where τ_f is the response time of the flow and τ_p is the response time of the particle. If the Stokes number is less than 1 then the particles will have enough time to adjust to the change in the flow path around an object [29]. This means that the particle and fluid will have nearly identical velocities and the particles stay entrained in the mainstream flow thus avoiding interaction with the coolant fluid. When the Stokes number is greater than 1 the particles will not have enough time to fully adjust to the change in the flow velocity and will continue on their own inertial characteristics. When this happens the particles will begin to interact with both the main coolant jet and the secondary flows that form downstream of the cooling holes, and may impact the test article surface.

Stokes numbers were calculated for the mean particle diameter for the engine and laboratory conditions shown in Table 4.1. For this analysis, it was assumed that particles were traveling with the same velocity as the mainstream hot gas path. The engine mainstream velocity, U_∞ = 150 m/s, was calculated assuming a turbine inlet Mach number of 0.2 and a turbine inlet temperature of 1509 K [30].

Table 4.1. Stokes Number Conditions

	Laboratory	Engine
Mainstream Temperature, T_∞ (K)	1339	1509 [30]
Fly Ash Density [3], ρ_p (kg/m^3)	1980	1980
Cooling Hole Diameter, d (mm)	4.0	0.5
Mainstream Velocity, U_∞ (m/s)	66	150
Mainstream Viscosity, μ	4.9×10^{-5}	5.3×10^{-5}
Median Particle Size, $d_{p,med}$ (μm)	13.0	3.2
Median Particle Stokes Number, Stk_{med}	6.3	6.3

Figure 4.3 shows the Stokes number vs. particle diameter with respect to fly ash particle diameter for engine and laboratory conditions. The reference lines in Figure 4.3 show that 13 μm particles in the laboratory have approximately the same Stokes number as 3.2 μm particles in the engine based on the previous assumptions. Although the exact distribution of particle sizes that exist in actual engine conditions is unknown, all particles greater than 10 μm and most particles greater than 1 μm are removed by modern filtration systems [6]. The Stokes similarity at engine conditions would be approximately equivalent to a 3 μm particle which is within the expected range of an actual industrial gas turbine. The Stokes analysis presented here shows that particle inertial characteristics can be matched between engine and laboratory conditions for the limiting assumptions made herein. It was concluded based on this analysis that the Stokes number was high enough for the particles to interact with the coolant flows and thus was not the cause of the lack of deposition on the test articles.

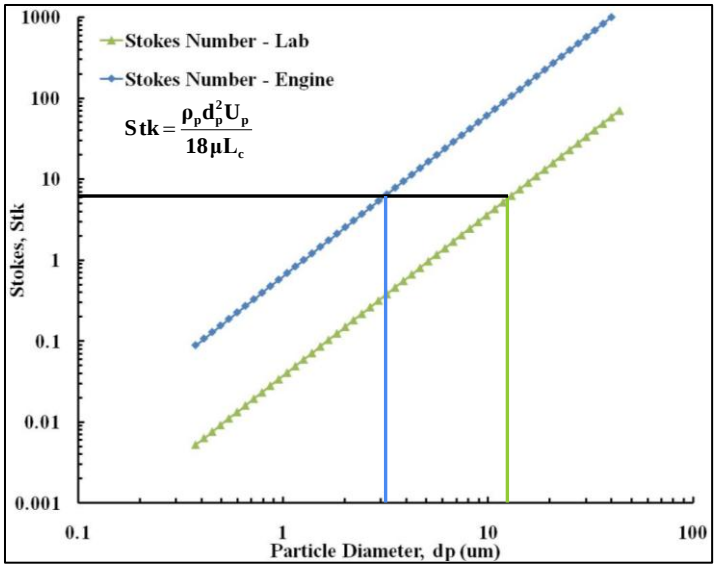

Figure 4.3. Stokes number vs. particle diameter between engine and laboratory conditions.

4.3 Particle Injection Analysis

Another concern for the lack of deposition on the initial run of the test articles was whether the particles were being injected deep enough into the flow. With the new injection tube complete, an analysis was performed to examine how deep the fly ash would penetrate into the flow. An analysis of the injecting streams interaction with the mainstream cross flow was performed using a method described in Hautman et al. [31]. Their work developed three correlations to measure how deep the flow would inject into the cross flow based on momentum ratio, MR, and the distance downstream from the hole. These correlations can be seen below in Equations 4.3, 4.4, and 4.5.

$$Y_{min}(Z) = 0.31 * d_{tube} * MR^{0.5} \left(\frac{Z}{d_{tube}}\right)^{0.33} \tag{4.3}$$

$$Y_{mid}(Z) = 0.56 * d_{tube} * MR^{0.5} \left(\frac{Z}{d_{tube}}\right)^{0.33} \tag{4.4}$$

$$Y_{max}(Z) = 0.73 * d_{tube} * MR^{0.5} \left(\frac{Z}{d_{tube}}\right)^{0.33} \quad (4.5)$$

It is important to note that this analysis was performed in a two dimensional cross flow. It was not intended to be completely accurate but more as a reference point for how far the particles would penetrate into the flow. The particles in the combustion facility experience a swirl effect which changes their momentum and reduces penetration depth. A plot was created that allowed the penetration depth to be compared to the distance downstream of the injection point. This analysis showed that the particulate matter was injecting too far into the channel and was impacting the opposite wall. The objective was to have the flow inject into the hot gas path but not through it. To reduce the flow momentum the injection tube was raised by 1.5 inches to allow the port area to increase thus reducing the flow velocity. Lowering the exiting velocity allowed the flow to penetrate into the middle of the hot gas path but not all the way across the channel.

Plotting the injection depth against the distance from the injection point is displayed below in Figure 4.4. Figure 4.4 was developed in MathCAD (see Appendix A for equation code) and is displayed in meters.

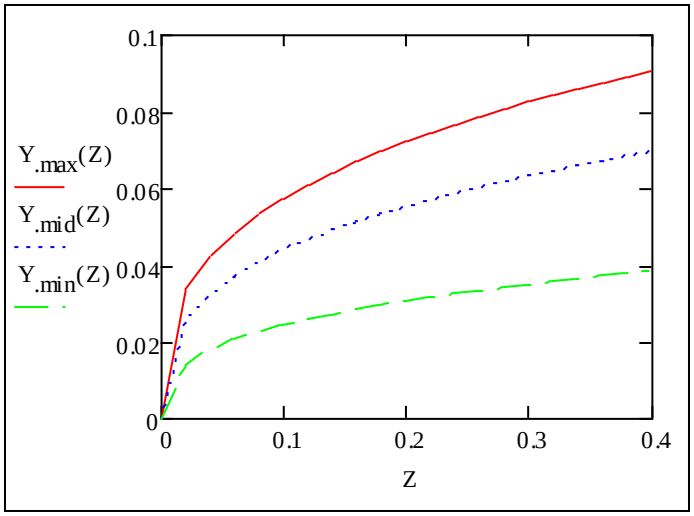

Figure 4.4. Injection depths of Nitrogen line into the cross flow vs. distance from injection point downstream.

4.4 Thermal Equilibrium Analysis

In order to ensure that particles reached the flow temperature and would soften or become molten, similar conditions in a gas turbine, the particles need to be at thermal equilibrium before they encountered the test article. A lumped mass analysis was performed to evaluate whether the particles would be at thermal equilibrium before they impacted the test article. The particle temperature equation was taken from *Introduction to Heat Transfer* [32] and is seen below in Equation 4.6.

$$T_P = (T_i - T_\infty)e^{\left[-\left(\frac{hA_s}{\rho_p Vc}\right)t\right]} + T_\infty \tag{4.6}$$

Two unknowns in the above equation were t, time, and h, heat transfer coefficient. To calculate a value for h, Equation 4.7 was used [31].

$$Nu_d = 2 + 0.6Re_d^{1/2}Pr^{1/3} \tag{4.7}$$

A no slip condition was applied causing Re_d to become zero and the Nu_d to have a value of 2. A no slip condition would be the "worst case" scenario for determining whether the particles would reach thermal equilibrium because it eliminates the convective effects of the flow which would be extremely large due to the high freestream velocity in the facility. Using the value of Nu_d; h was calculated using Equation 4.8.

$$Nu_d = \frac{hd_p}{k_f} \tag{4.8}$$

The time required to reach thermal equilibrium was calculated using the value of h from Equation 4.8. Displayed below in Figure 5 is the graph showing the time required to reach thermal equilibrium for different particle diameters. The mean particle diameter of the processed fly ash was 13 μm. Examining the plot it can be seen that at the mean particle diameter reached thermal equilibrium in less than 1/100 of a second.

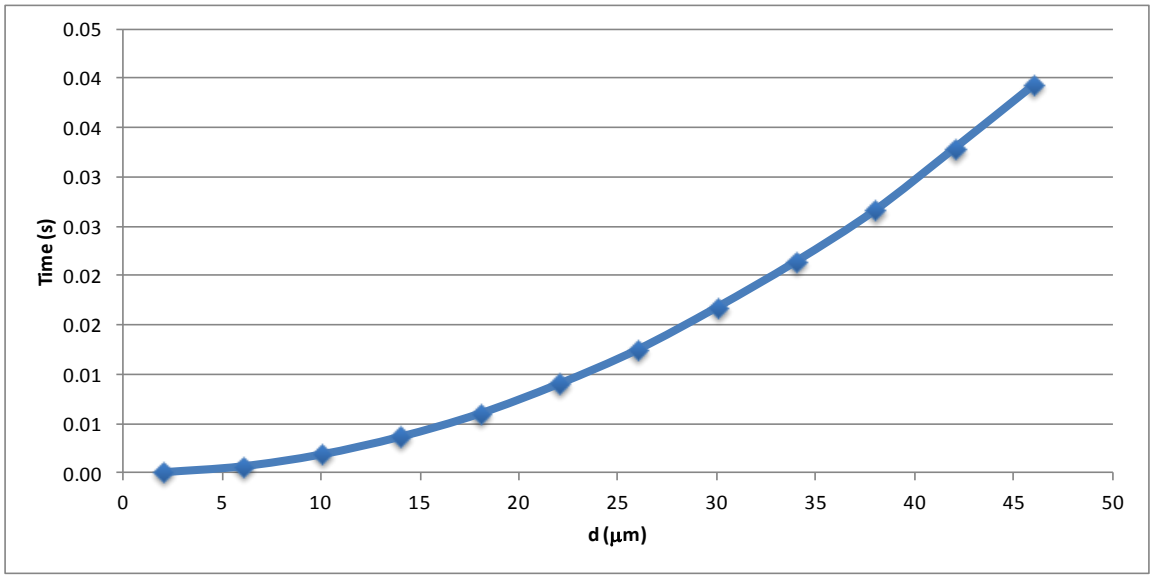

Figure 4.5. Plot of particle diameter vs. time required to reach thermal equilibrium.

An important value to know was the distance that would be required for the particles to reach thermal equilibrium. The test article sits approximately 33 cm downstream of the injection point. Therefore, the majority of the particles needed to be at thermal equilibrium so that they would be molten before they impact test article. Figure 4.6 displays the graph of the particle diameter vs. the length required to reach thermal equilibrium.

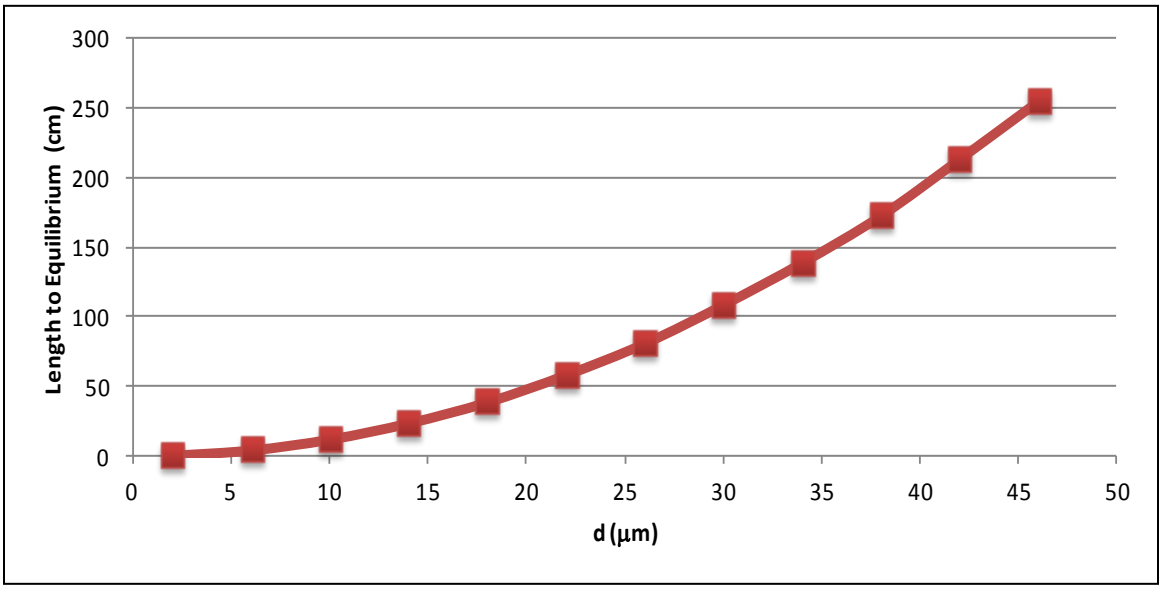

Figure 4.6. Plot of the particle travel vs. diameter distance required to reach thermal equilibrium.

As the particles approach 20 μm in diameter the length it takes to reach equilibrium was past the test article. However, it should be noted that over 80% of the particles had smaller diameters and would have reached thermal equilibrium before impacting the test article. Another important factor is that this thermal analysis was performed to model the "worst case" scenario where no convection was considered moving around the particles. In reality the particle would have a very high convection coefficient due to the high velocity of the mainstream flow going around the particle. Therefore, the method that was described above was considered a conservative approach and all particles were most likely at thermal equilibrium before they

impacted the test article. Due to this conclusion the effects of the particles not reaching equilibrium was ruled out as a possibility for the lack of deposition in initial tests.

The analyses did not provide any indicators that would cause the lack of deposition that occurred during initial tests. A hypothesis was formed that the surface temperature of the test article was not hot enough to allow particulate deposition. The theoretical sticking temperature reported in Webb et al. [20] was not applicable to the current study. The TuRFR used actual aircraft egine turbine doublets. The doublets were film cooled but did not have any other cooled surfaces around them. The test article in the current study was film-cooled and was also situated in a water-cooled holder that would result in a lower surface temperature at the same freestream temperature conditions. Based on this hypothesis all future testing was conducted at temperatures higher than 2000 ^{o}F.

4.5 Development of Surface Temperature Measurement

A system was developed to measure the surface temperature of the test article using a method of two equations and two unknowns. The two unknowns would be the reflective temperature of the surrounding walls and the surface temperature of the test article. The assumption was made that if two points were selected that were close to each other the wall temperature would be common between them. The two locations needed to have one in the trench region and the other in the TBC region. These two regions will have different emissivities. Figure 4.7 displays the test article and the basis for the analysis. For distinction the subscript 1 will represent the bare metal of the test article cooling trench. The subscript 2 represented the TBC layer. For more detail on this process see *Introduction to Heat Transfer* [32].

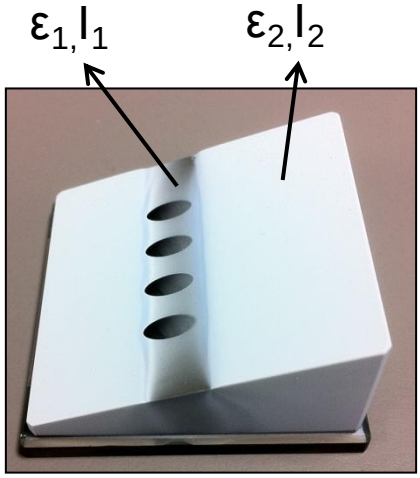

Figure 4.7: 20^{o} TBC coupon and its two reflective surfaces

Equation 4.9 and 4.10 represent the equations that calculated the intensity for each point. Two components made up each equation; intensity of the face, I_{BB}, and the reflected intensity of the surrounding walls, I_W.

$$I_1 = \epsilon_1 I_{BB}\tau + (1-\epsilon_1) I_W \tau \tag{4.9}$$

$$I_2 = \epsilon_2 I_{BB}\tau + (1-\epsilon_2) I_W \tau \tag{4.10}$$

By setting the equations equal to each other based on I_W being equal a value for the I_{BB} can be calculated as seen below in Equation 4.11.

$$I_{BB} = \frac{(1-\epsilon_2)I_1 - (1-\epsilon_1)I_2}{(1-\epsilon_2)\tau\epsilon_1 - (1-\epsilon_1)\tau\epsilon_2} \tag{4.11}$$

The values for I_1 and I_2 can be calculated using Plank's Law as seen below in Equation 4.12. Since only a single wavelength was used the equation was only a function of temperature.

$$I(T) = \frac{2hc_o^2}{\lambda^5\left[e^{\left(\frac{hc_o}{\lambda kT}\right)} - 1\right]} \tag{4.12}$$

The assumption that the exponential was much greater than 1 was used and the equation was rearranged to solve for the temperature with I(T) being I_{bb} resulting in Equation 4.13.

$$T = \left(-\frac{hc_o}{\lambda k}\right) \Big/ \ln\left(\frac{I(T)\lambda^5}{2hc_o^2}\right) \tag{4.13}$$

Based on this method the surface temperature could be calculated assuming that everything was constant during the process. However, upon further inspection the transmissivity was found not to be constant but actually be a function of time and the mainstream gas temperature. The inner quartz window began to devitrify (change phase) almost immediately and continued to become more opaque as the test time increased. Another issue was the emissivity which also changed as the test time increased and deposits were deposited onto the test article.

At the time this thesis was written there was not a viable solution to these problems. Another solution was proposed by researchers at NETL to use a single wavelength camera measurement technique. The transmissivity would be measured in a lab for all of the optics, and the emissivity would be measured by taking an image of the test article with an IR light source on and without the IR source. By dividing the intensities recorded in these images a reflectance can be calculated. Using the reflectance and the transmissivity the emissivity can be calculated. A black body source will be used to calibrate the intensity that the camera is registering to the known intensity of the black body. Finally, a point measurement will be taken using a sensor on

the surface of the test article to get a value for the surface temperature. With these values a reflected intensity can be ascertained and a value for the surface temperature at those conditions would be available [33].

CHAPTER 5:
Main Testing Phase Results and Discussion

5.1 Test Plan

The original test plan was going to examine the evolution of deposit growth on the two test article geometries at two different blowing ratios. However, limitations in the facility resulted in an alteration of the test plan. Originally, the test articles were going to be scanned between two 3-hour runs. The presence of the "sluffing" or detachment of most of the deposit structures forced the test time for each to be reduced to 3-hours however one 6-hour test was performed. The particulate loading was not increased because of the limitations in the amount of fly ash that the seeder could contain. A small sampling of tests displayed deposition that was resistant to the "sluff" that occurred after cool down. Roughness characteristics for those cases are displayed in the appropriate sections. The presence of a large flow alteration caused by the swirl exiting the combustor region was evident in all results shown below. To combat the effects of the swirl, described in the following sections, the test plan consisted of altering one variable during each run to try to induce more deposition on the face. At the end of these runs comparisons were made looking at the 5 different factors.

A theoretical sticking temperature of 1950F [20] has been reported for fly ash of a similar composition to the fly ash obtained for this study. This temperature had already proven to not be hot enough for the current testing due to the shakedown testing being performed at 2000^{o}F. This study increased the temperature until deposition began to form and then increased it again to compare how the freestream temperature affected the amount of deposition. Previous studies found that more deposition occurs on objects that create a greater obstruction in the flow. Tests were performed with test article face angles of 10^{o} and 20^{o} to study the effects of impaction angle on deposition. The effects of blowing ratio were going to be studied at values of 1.0 and

2.0, respectively in the original test plan. Due to limitations onsite the maximum blowing ratio that was attained was 1.0. It was concluded that it would be sufficient to study the blowing ratio effect from 0.0, 0.25, and 1.0. Previous studies examined the effects of TBC versus bare metal on the growth of deposits and showed that deposition formed on TBC in larger concentrations than on bare-metal. Tests were performed at the same conditions with and without TBC to determine the effects of thermal barrier coating on deposition growth. The particulate loading parameter was varied by increasing the test duration while holding particulate concentration constant at 33 ppmw. The subsections that follow will display images taken during the run, after the run and explain the results found. In summary, the five main factors of deposition that were examined were:

- Freestream Temperature
- Impaction Angle
- Blowing Ratio
- Particulate Loading
- Surface Coating (TBC vs. non-TBC)

5.2 Free Stream Temperature Effects

The effects of free stream temperature on deposition growth were examined on a 20^{o} test article with a blowing ratio of M=1.0. Some deposition formed intermittently during the test at 2200^{o}F. These deposits are shown in Figures 5.1a-5.3a. Figure 5.3a is an image taken from the camera system attached to the high pressure facility. The distortion of the image is a result of devitrification of the internal sight glass. The mainstream temperature was increased from 2200^{o}F until deposition started forming on the surface of the test article. At a temperature of

approximately 2315^{o}F the particles started to adhere to the surface more rapidly. Figures 5.1b-5.3b display images of the tests run at 2315^{o}F. Figure 5.3b is an image taken with the black and white camera and has a similar devitrification pattern. The camera images are the last frame of a time lapsed video created for each run. Appendix E displays frames from an entire 3-hour test to show the evolution of the deposits.

Deposition only occurs on one side of the test article which was the first sign of the issue of the large swirl effect exiting the combustor region. This will be discussed in a later section. Deposition occurred on the back side of most of the cooling holes. The holes closer to the side with deposits had more in deposition. The deposition that did occur was not significant but it was not expected due to the high blowing ratio of the cooling holes.

The results of the freestream temperature study showed that as the temperature increased the deposition increased. This result was consistent with work performed in previous studies by Jensen et al. [10], Crosby et al. [14], and Webb et al. [20]. An important note about the freestream temperature was the theoretical sticking temperature difference between the work being performed here and the work performed in the literature. Specifically, Webb et al. [20] reported a theoretical sticking temperature of approximately 1950^{o}F. After performing experiments at 2000^{o}F and not getting deposition the results of this study showed that the sticking temperature was around 2200^{o}F. The difference between the temperatures may be due to the experimental setup or the fly ash particle size and composition. Webb et al. used aircraft turbine doublets for the test components rather than industrial gas turbine components. The doublets were film-cooled but not backside cooled, such as the test articles in the current study. The current study used a test article that was housed in a water cooled holder. The water cooling would theoretically cool down the test article more than the doublets which would require a

higher freestream temperature to create an environment conducive to deposition. The doublets were also being heated on both sides while the face of the test article in this study was being heated on the front side and backside cooled with a water-cooled jacket surrounding it. These differences may have contributed to the difference in the theoretical sticking temperature. The TuRFR used in [20] is designed to use aircraft components as the test articles. The size difference between the particle diameter and the cooling holes is much greater which would result in the cooling holes being less effective in resisting deposition.

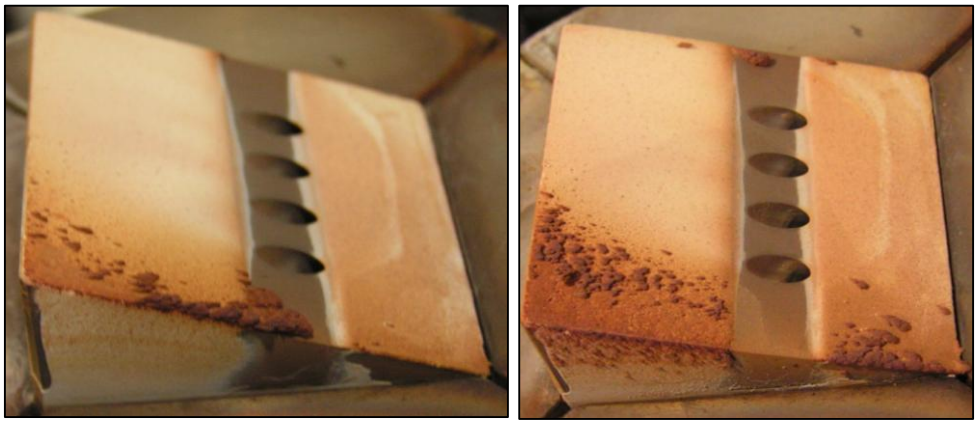

(a) (b)

Figure 5.1. Side view of deposition at mainstream temperature of (a) 2200^{o}F and (b) 2315^{o}F on a 20^{o} angle test article.

(a) (b)

Figure 5.2. Top view of deposition at mainstream temperature of (a) 2200^{o}F and (b) 2315^{o}F on a 20^{o} angle test article

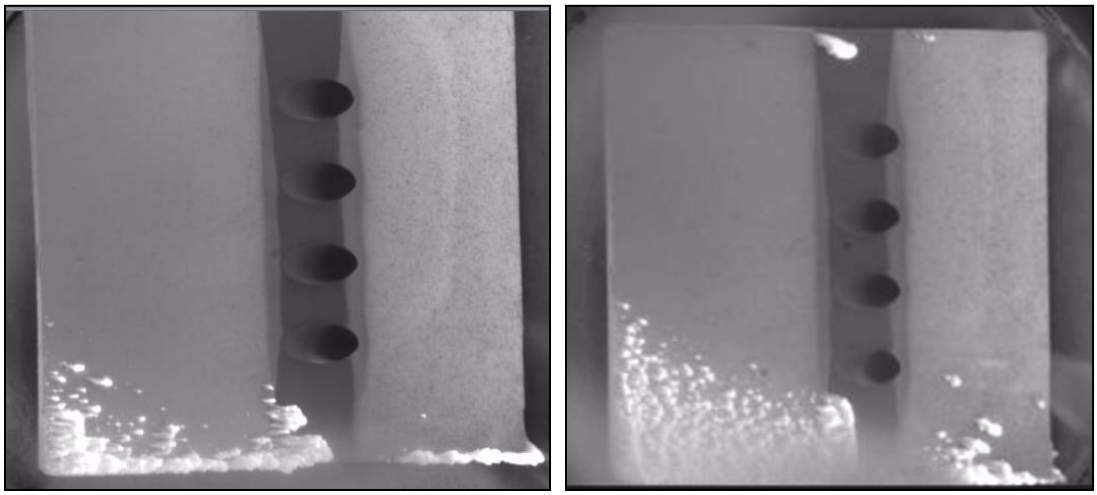

(a) (b)

Figure 5.3. Black and white camera view from side view port of deposition at mainstream temperature of (a) 2200°F and (b) 2315°F on a 20° angle test article.

Figure 5.4 displays the area that roughness scans were performed on. This image differs from the image taken from the camera due to some of the deposits sluffing off. Table 5.1 displays the roughness characteristics recorded by the LEXT software that came with the microscope. Due to the particles in the study being approximately 3X larger than the particles in actual gas turbines the roughness characteristics were scaled to match the mean particle diameter scaling. Webb et al. [20] measured the thickness of their deposits as a percentage of the thickness in mm by the particulate loading (ppmw-hr). The study presented the percentage thickness as approximately 0.009 (mm/ppmw-hr) for midspan at 37% chord of the vane. For the current study the area that was studied was closer to 10-20% chord but a comparison showed that percentage thickness was approximately 0.012 (mm/ppmw-hr).

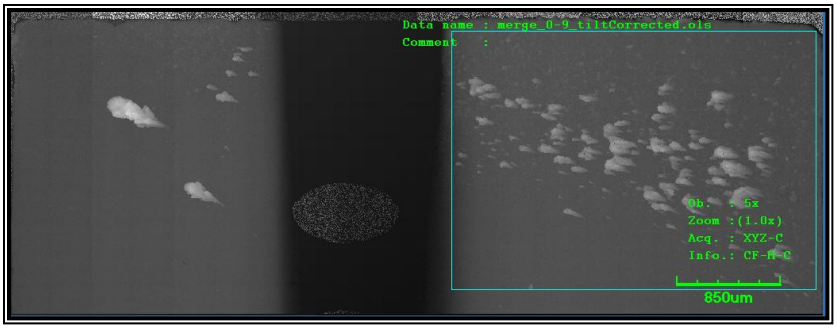

Figure 5.4. Image of deposition that was scanned for roughness characteristics for 20° test article at freestream temperature of 2315°F.

Table 5.1. Roughness Characteristics Freestream Temperature 2315°F.

Parameter	Description of Roughness Parameters	Height (μm)
SRp	Maximum Peak Height	246
SRv	Maximum Valley Depth	156
SRz	Avg Maximum Height	402
Sra	Roughness Average	17
SRq	Root Mean Square Avg	29

5.3 Test Article Face Angle Effect

The effect of the two different test article face angles was examined in two different studies. The first study was performed at the original 2200°F mainstream temperature with a blowing ratio of M=1.0. The results showed very little deposition on the 10° test article except along the edge. Figures 5.5-5.7 display the 10° test article with 5.7 showing a camera image comparison of the 10° test article and the 20° test article at the same conditions. The 20° test article accumulated more deposition; which was expected due to it being more of an obstacle in the flow.

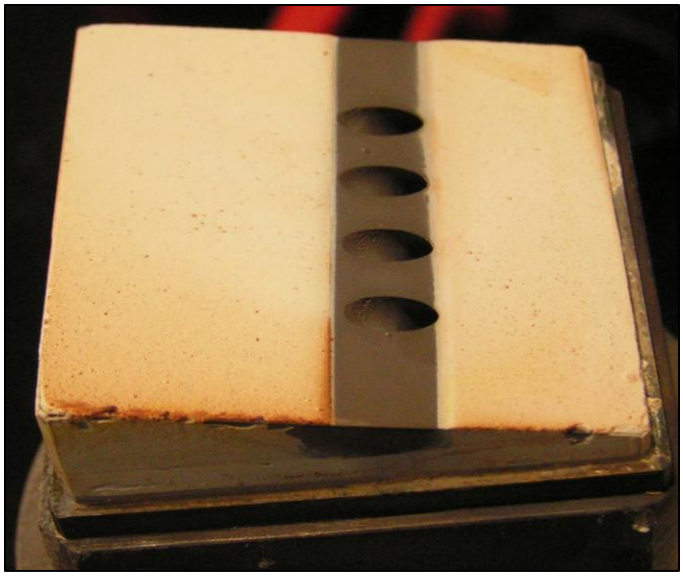

Figure 5.5. Side view of deposition at mainstream temperature of 2200^{o}F on a 10^{o} angle test article at M=1.0.

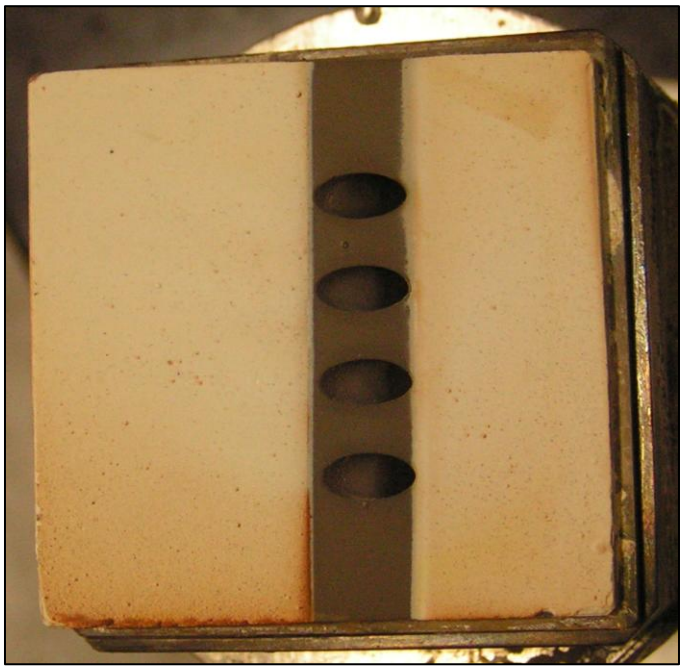

Figure 5.6. Top view of deposition at mainstream temperature of 2200^{o}F on a 10^{o} angle test article at M=1.0.

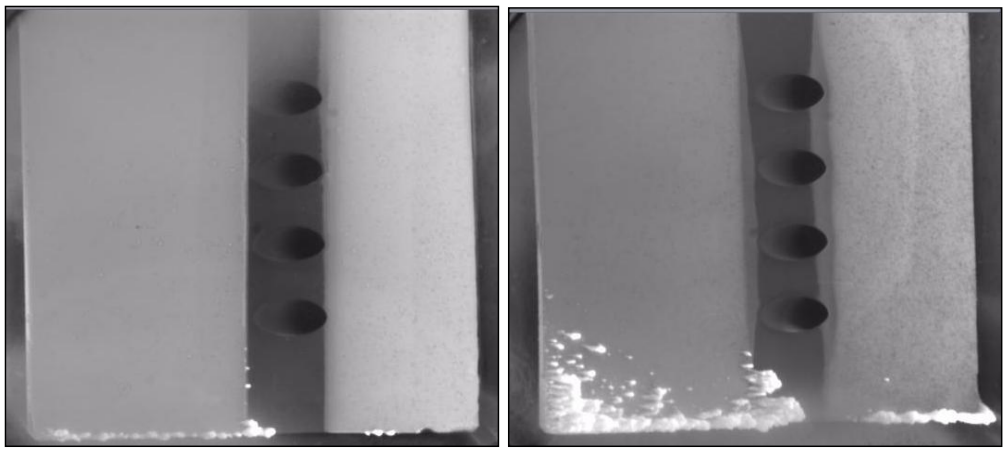

(a) (b)

Figure 5.7. Comparison of (a) 10^o and (b) 20^o test articles at M=1.0 and a freestream temperature of 2200^{o}F.

Another comparison between the test article face angles was performed at the elevated operating temperature of 2315 ^{o}F and a blowing ratio of M=0.25. Figures 5.12a-5.14a display the 10^o test article with 5.14 being the camera image. More deposition formed inside the cooling holes at the lower blowing ratio. Figures 5.12b-5.14b display the 20^o test article. Similarly to the higher blowing ratio and lower operating temperature case the steeper the angle obstructs the flow the more deposition formed on it. All of these test articles display the effects of the swirl from the combustor and only have deposition formed on one side of the test article face. All facility camera images display the devitrification that occurred during testing on the interior sight glass.

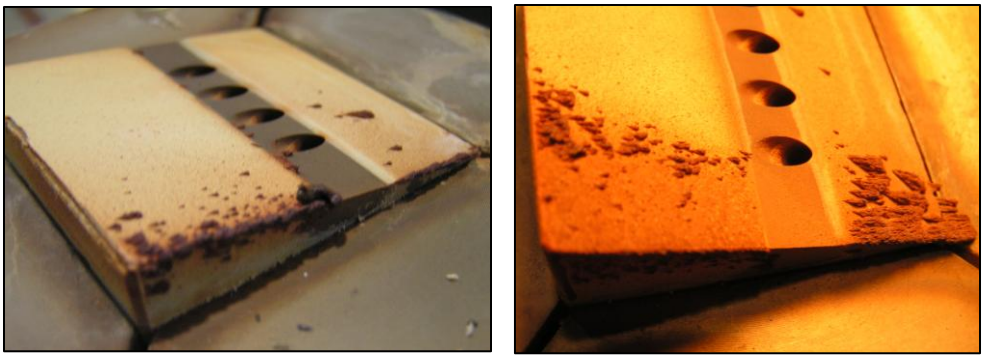

(a) (b)

Figure 5.8. Side view of deposition at mainstream temperature of 2315°F on a (a) 10° and (b) 20° angle test article at M=0.25.

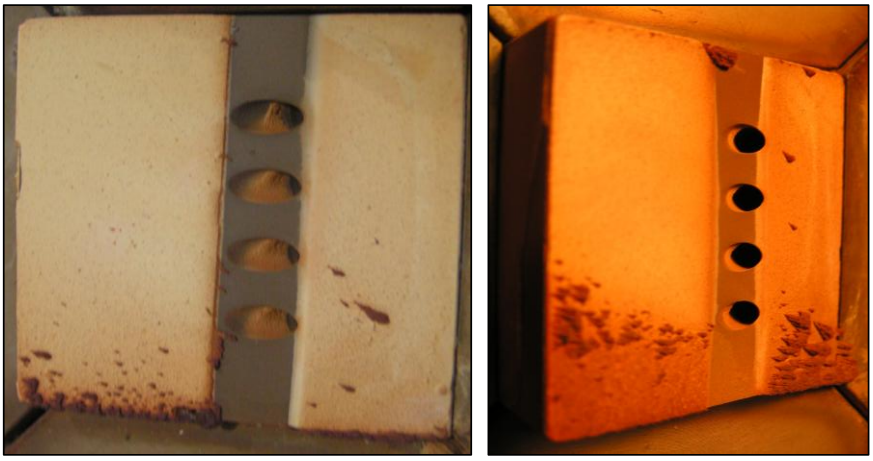

(a) (b)

Figure 5.9. Top view of deposition at mainstream temperature of 2315°F on a (a) 10° and (b) 20° angle test article at M=0.25.

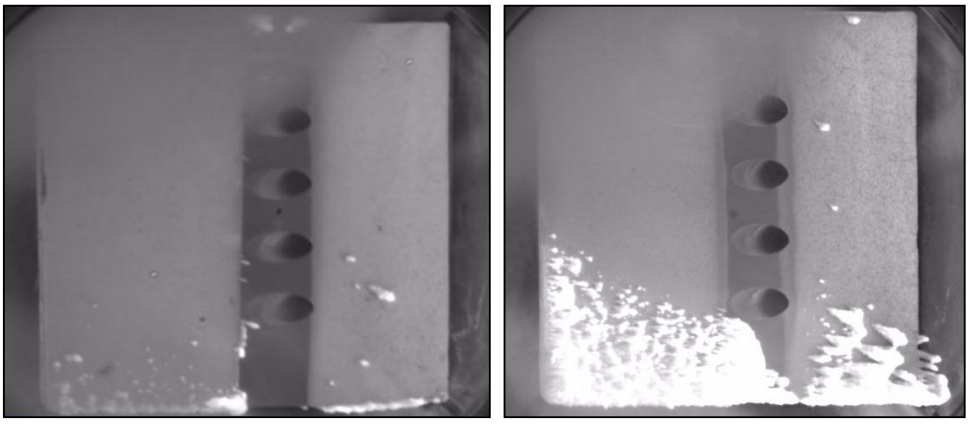

(a) (b)

Figure 5.10. Black and white camera view from side view port of deposition at mainstream temperature of 2315°F on a (a) 10° and (b) 20° angle test article at M=0.25.

This result was consistent with work performed by Jensen et al. [10] in the respect that their results also showed the increase in deposition as the impaction angle increased. The results of their study and the current one were consistent with the results reported by Bons et al [9] with the leading edge displaying large deposition structures due to the impaction angle being close to 90^{o} in relation to the flow path. The results also agree with work performed by Laycock and Fletcher [19] whose findings showed that the increase in impaction angle would result in an increase in deposition.

5.4 Blowing Ratio Effects

Blowing ratio (mass flux of coolant jet/mass flux of freestream flow) effects on the blade were examined at 45 psig operating pressure and 2315^{o}F operating freestream temperature, using the 20^{o} test articles. Originally, blowing ratios of M=1.0 and M=2.0 were going to be used to perform the experiments. However, the facilities at NETL could not produce blowing ratios of above M=1.0 so the plan was adjusted. Tests were performed with blowing ratios of M=1.0, 0.25 and finally 0.0. The case of M=0.0 was still back side cooled. The cooling holes were covered with a metal plate to prevent cooling air from exiting out of the cooling holes. Figures 5.11 and 5.12 below display the test article after the M=0.0 blowing ratio case. This case had more deposition across the entire face than the rest of the cases performed during this project. Specifically the area where the trench rises from the cooling holes was approximately 80% covered. The cooling holes showed significant deposition build up and the initial stages of blockage. Figure 5.13 displays the comparison between the blowing ratios of M=0.0, 0.25 and 1.0. The accompanying photos for the cases of 0.25 and 1.0 were shown in a previous section. The effects of the swirl were apparent on all of the test articles. The M=0.0 case had more

coverage but the deposition started on the same side and grew across the test article. As the blowing ratio increased the amount of deposition on the face and in the holes decreased. There was no significant deposition in the cooling holes of the M=1.0 case.

The variation of cooling blowing ratio affected deposition significantly. As the blowing ratio increased from M=0.0 to 1.0 the amount of coverage of the deposition decreased significantly. These findings concur to the studies by [15], [7], and [16]. At the blowing ratio of 0.0 (i.e. no cooling) the entire trench and cooling holes were covered by deposits. The cooling holes were not completely blocked but had started to be covered. At a blowing ratio of 0.25 there was some evidence of deposits in the cooling holes. However, at the highest blowing ratio of 1.0 there was no evidence of deposition in the holes. These results appear to agree with the work of ([16], [17]) that the cooling jets both deflect smaller particles away and lower the surface temperature of the component to reduce the overall amount of deposition.

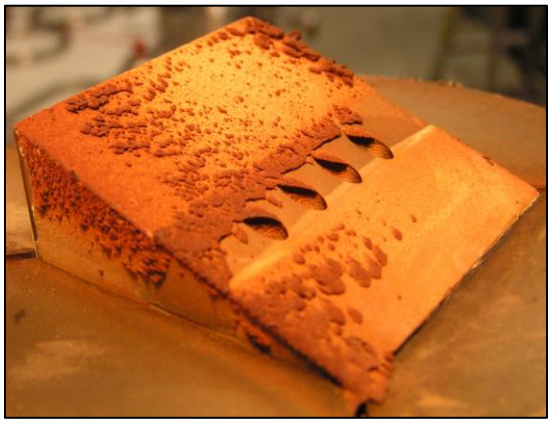

Figure 5.11. Side view of deposition at mainstream temperature of 2315^{o}F on a 20^{o} angle test article at M=0.0.

Figure 5.12. Top view of deposition at mainstream temperature of 2315°F on a 20° angle test article at M=0.0.

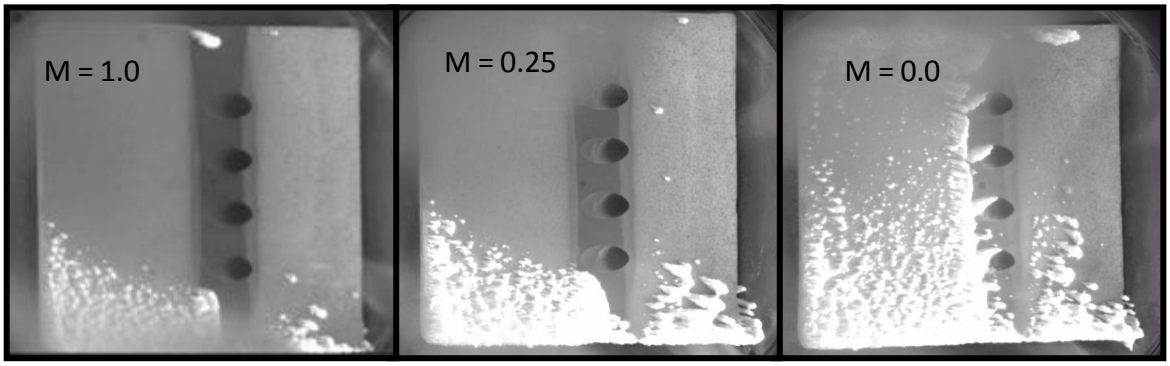

(a) (b) (c)

Figure 5.13. Comparison of blowing ratio effects on 20° test article at a free stream temperature of 2315°F (a) M=0.0, (b) M=0.25, and (c) M=1.0.

5.5 Effects of Different Particulate Loading

A study was performed to examine the effects of varied particulate loading on deposition. To vary the particulate loading from 100 ppmw-hr to 200 ppmw-hr the test time was increased from 3 to 6 hours. As with previous tests, the pressure was at 45 psig and the temperature was 2315^{o}F. The blowing ratio was set to M=1.0. Figures 5.15-5.16 display the results of the 6-hour test. These images were compared to the results of the same conditions during a 3-hour test in Figure 5.17. The patterns of the deposition were both similar however the 6-hour test had significantly more deposition than the 3-hour test. It should be noted that the dark lines that appear on the camera image in Figure 5.16 were scratches on the interior view port. The deposition of the 6-hour test dislodged but remained intact so an adhesive was applied to the material and it was reattached to the surface. A surface roughness scan was taken of the deposition. The scan is shown in Figure 5.18 and the roughness characteristics are shown in Table 5.2. The roughness characteristics were scaled based on particulate mean diameter to compare with data in the open literature. Table 5.2 displays both the results of the 6-hour test and the 3-hour test for comparison. The 6-hour test showed an increase in surface roughness over the 3-hour test. Raw data of the scan results can be found in Appendix B.

The difference in particulate loading simulated test or exposure time also displayed a significant impact on formation of deposition. A more detailed view of the roughness characteristics is shown below in Figure 5.14. The blue line represents the mean average roughness line and y_i represents the measurements to the peaks and valleys used for the centerline averaged roughness and RMS roughness calculations as defined in Equations 2.1 and 2.2, respectively. SRp and SRv define the distance from the centerline to the highest peak and

lowest valley, respectively. Adding SRp and SRv together would produce the value SRz, the maximum peak-to-valley distance.

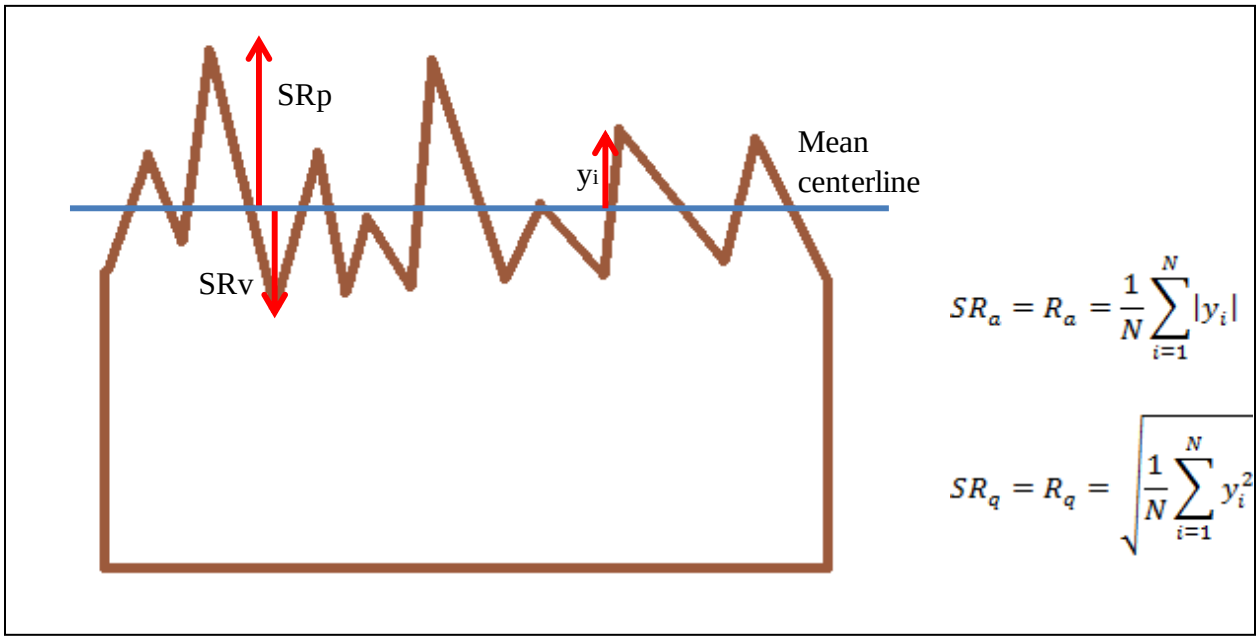

Figure 5.14. Schematic of roughness heights

The SRp and SRv difference between the 3-hour run and 6-hour run increased by 62% and 132%, respectively. The Sra or average roughness increased by 365% while the RMS averaged roughness increased by 240%. The increase in Sra was much larger than the increase reported in Wammack et al. [17] which reported an increase of approximately 50%. In the current study the Sra value increased from 17 to 79 μm while in [17] the increase was from 10 to 15 μm. The value of SRz which increased by 91% (from 402 to 766 μm) in the current study only had a slight increase of 25% (from 12 to 15 μm) in the previous study. These results differ from findings of Wammack et al. [17] where a "lull" in the deposition growth was discovered. In the current study, no lull was discovered as the roughness of the deposits continued to increase during the same simulated operating conditions. One difference that should be noted is that the

particulate concentration (20 ppmw) and mean particle diameter (15 μm) were different than the 33 ppmw and 13 μm particle diameter of the current study.

The increase in deposition over the course of the run time is consistent with the findings of Ai et al. [15] that showed the same results. Their results showed that the capture efficiency increased as the operating time increased and that the changes in roughness patterns that occur during the deposit structure growth. The patterns showed distinct patterns followed by periods where the deposits filled in the valleys. Lawson and Thole [12] reported a point in their study when the deposition process reached an apparent state of equilibrium (i.e. no additional increase of deposition was observed with increased exposure/run time). This study did not appear to reach an equilibrium point in the deposition process but the length of time may not have been sufficient to reach that point. The conclusion found in this study was that the deposition increased during a longer operating run time, however the deposition may still sluff off during cool down. The wax adhesion is very different from fly ash and would not allow for the simulation of material break off during cool down.

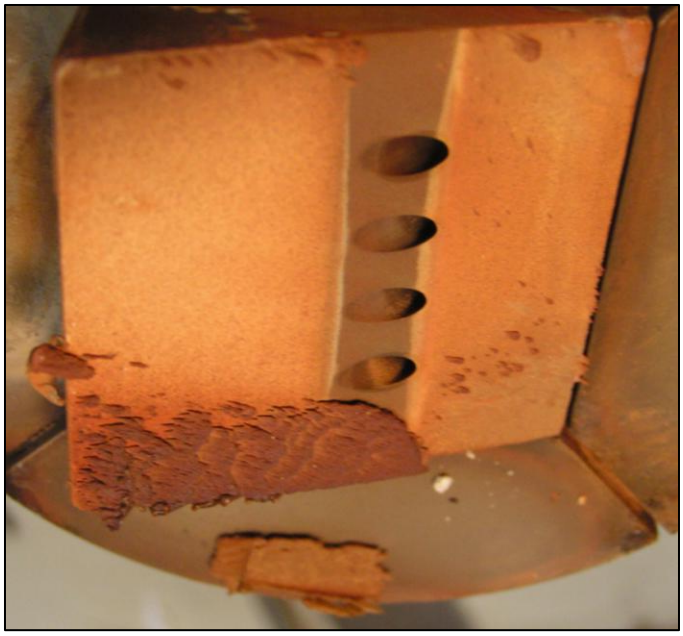

Figure 5.15. Side view of deposition at mainstream temperature of 2315^{o}F on a 20^{o} angle test article at M=1.0 for a 6-hour test.

Figure 5.16. Top view of deposition at mainstream temperature of 2315^{o}F on a 20^{o} angle test article at M=1.0 for a 6-hour test.

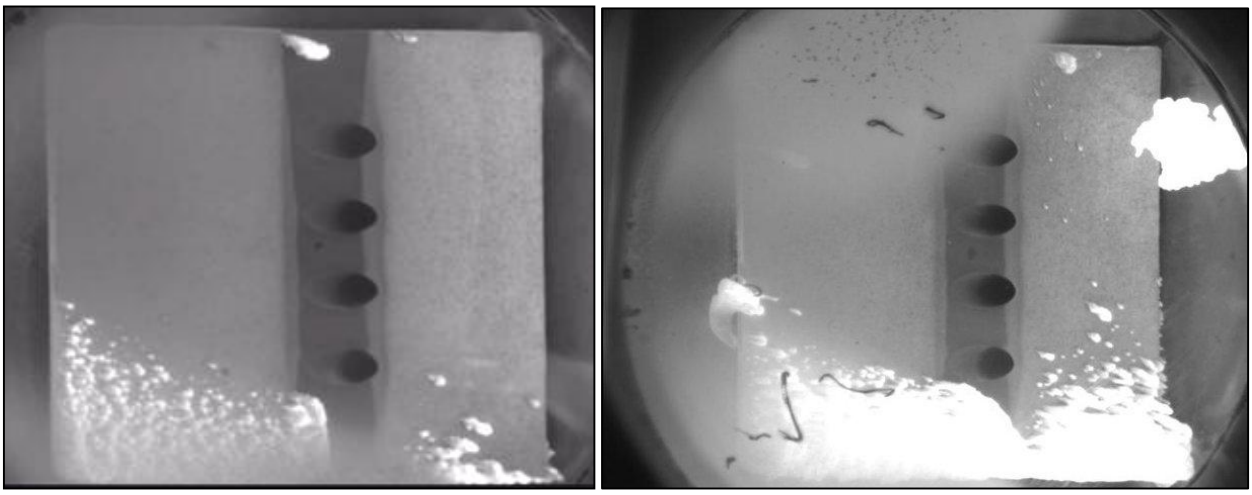

(a) (b)

Figure 5.17. Comparison between a (a) 3-hour run and a (b) 6-hour run at M=1.0 and a freestream temperature of 2315^{o}F.

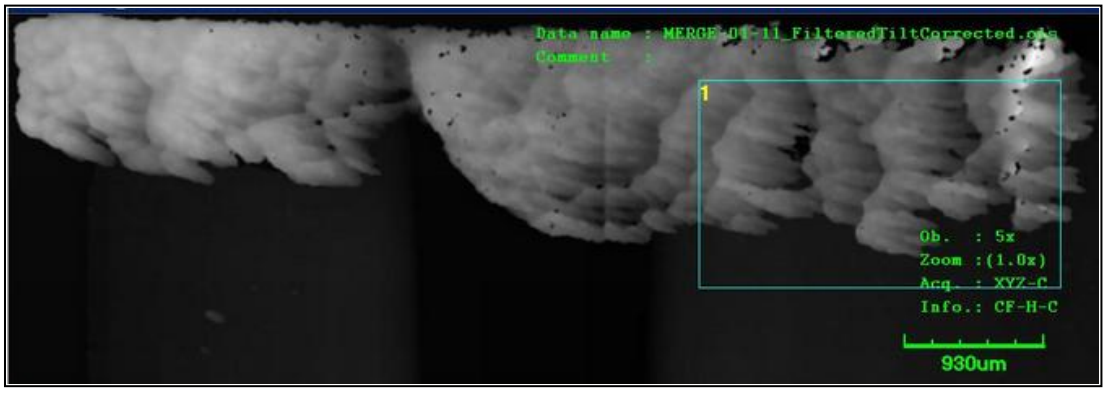

Figure 5.18. Selected area of deposition for 20^{o} test article at freestream temperature of 2315^{o}F for a 6-hour run.

Table 5.2. Roughness characteristics comparison of 20° test article at freestream temperature of 2315°F for a 3-hour (5,000 simulated hours) and 6-hour run (10,000 simulated hours).

Parameter	Description of Roughness Parameters	3-hour run Height (μm)	6-hour run Height (μm)
SRp	Maximum Peak Height	246	399
SRv	Maximum Valley Depth	156	367
SRz	Avg Maximum Height	402	766
Sra	Roughness Average	17	79
SRq	Root Mean Square Avg	29	100

5.6 Thermal Barrier Coating Effects

The effect of the thermal barrier coating (TBC) was examined by comparing a bare metal test article with a TBC coated test article. The tests were performed at a freestream temperature of 2315°F and a blowing ratio of M=1.0. Figures 5.19 and 5.20 display the results of the bare metal test article deposition. Very little deposition accumulated on the surface of the test article. It should be noted that the water in the corner of the images was due to some drips landing on it as the test article was being removed from the facility. Figure 5.21 displays a comparison of the bare metal and TBC test articles post-test. The TBC coated test article displays more deposition than the bare metal test article. The swirl effect was evident on the bare metal test article.

The differences between bare metal test article and the thermal barrier coated test article were similar to results found in the studies by Ai et al. [15], Wammack et al. [17], and Ai et al. [16]. The bare metal coupon resisted deposition which is consistent with previous studies such as Ai et al. [16], where it was found that at similar condition of blowing ratios and hole spacing that the capture efficiency (ratio of amount of deposition on coupon by the total injected deposition) was much higher for TBC coupons. In Bons et al. [9] the findings showed that regardless of the coating or non-coating the components would show signs of deposition. The

study does not however report on a direct comparison of how much deposition was found on a TBC coating to a bare metal coating. Ai et al [15] performed another study that found that the deposit structures on a TBC surface were on an order of magnitude higher than the structures found on the bare metal surface. The structures found on the TBC coated test article would agree with these results. However, the lack of any significant structures on the bare metal test article does contrast [15] and [9]. Wammack et al. [17] findings showed that bare metal test articles resisted deposition entirely for the first run (simulated 2500 operating hours). However, after the second run which simulated up to 5000 operating hours deposition had started to form on a small scale. The findings from the current study contradict this finding because the test article was simulated for 5000 operating hours and did not have any significant deposition on the face. The conclusion from this study was that the coating process (or lack of) does play an important role in the formation of deposits. TBC was much more susceptible to deposit formations than the bare metal counterpart although the deposits were prone to erosion as evidenced by the ease of the deposition sluffing off.

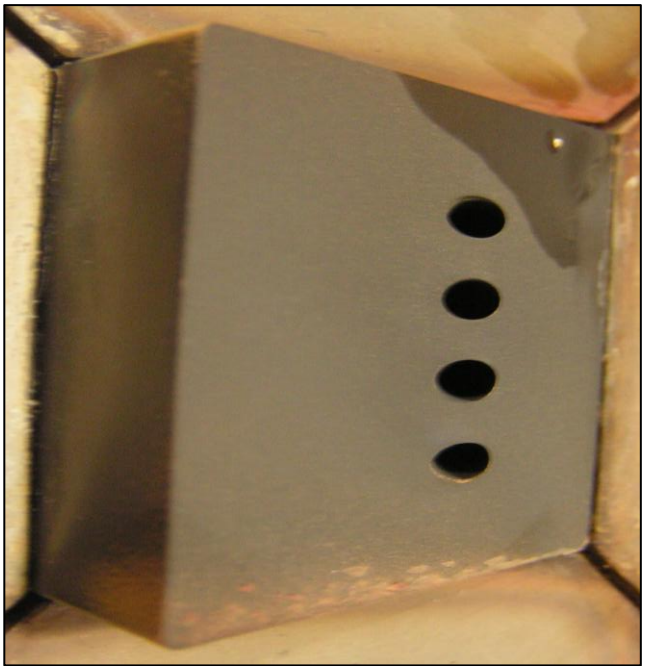

Figure 5.19. Side view of deposition at mainstream temperature of 2315^{o}F on a 20^{o} angle test article at M=1.0 without thermal barrier coating.

Figure 5.20. Top view of deposition at mainstream temperature of 2315^{o}F on a 20^{o} angle test article at M=1.0 without thermal barrier coating.

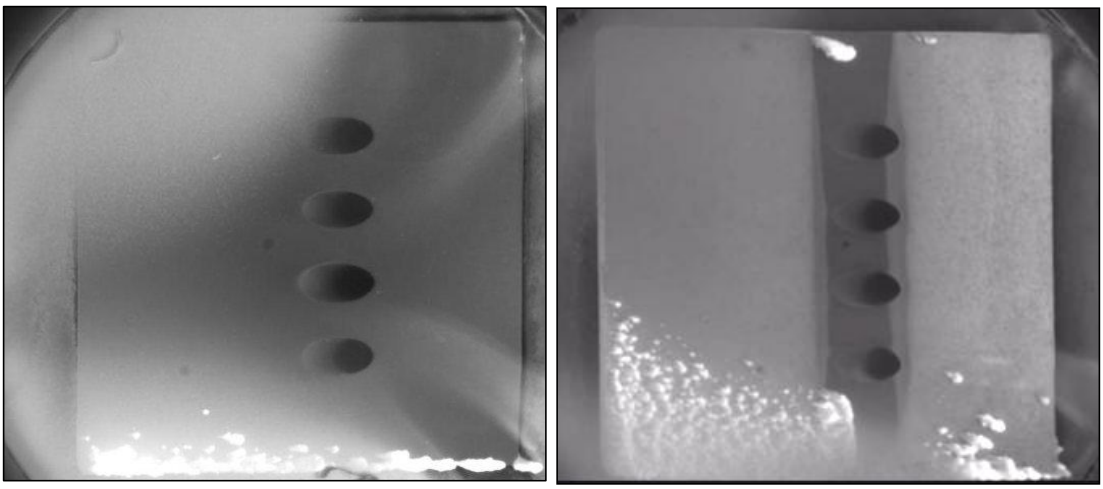

(a) (b)

Figure 5.21. Comparison between a test article that is (a) uncoated (bare metal) and a test article that has a (b) thermal barrier coating during a 3-hour test at a freestream temperature of 2315^{o}F and M=1.0.

5.7 Post-Testing Facility Teardown and Inspection

Following the conclusion of the testing the test section was torn down and an examination was performed to identify any areas of deposit structure growth on the interior walls surrounding the test article. Deposition was found to be covering all sections of the facility downstream of the injection point. A large structure had been developed on the transition piece at the entrance to the test section. This can be seen below in Figure 5.22 and a close up view in Figure 5.23. The growth was only on the left side of the transition piece and not on the right side. This growth displays the effect of the swirl that exits the combustor. The swirl turns counterclockwise and pulls the injection fly ash into the left side of the transition piece. The growth on the transition piece displayed below was on the same side of the aerothermal test section as the test articles.

Figure 5.22. Image of transition piece still attached to aerothermal test section displaying large structure of deposition build up.

Figure 5.23. Image of deposit structure on transition piece after removal from aerothermal test section.

There was significant deposition inside the channel, where large structures started to form in the area around the test article. Figures 5.23 and 5.24 display these structures from the upstream and downstream of the test section, respectively. These structures prove that although a large swirl effect was traveling through the channel there was enough flyash to create deposits on all four walls. Once the particles had traveled through the channel without sticking to any part they exited into the quench section coating all of the interior walls down the length of the quench section. These deposit growths certainly had an effect on the freestream velocity but

there was no way to measure that during the testing phase at NETL. Figure 5.25 displays the exit of the aerothermal test section coated in deposition. The cause of the deposition on all of the refractory walls was due to the high silica concentration in the walls at high temperatures being susceptible to reaction and deposition [34].

Figure 5.24. Image of deposit structure on transition piece after removal from aerothermal test section.

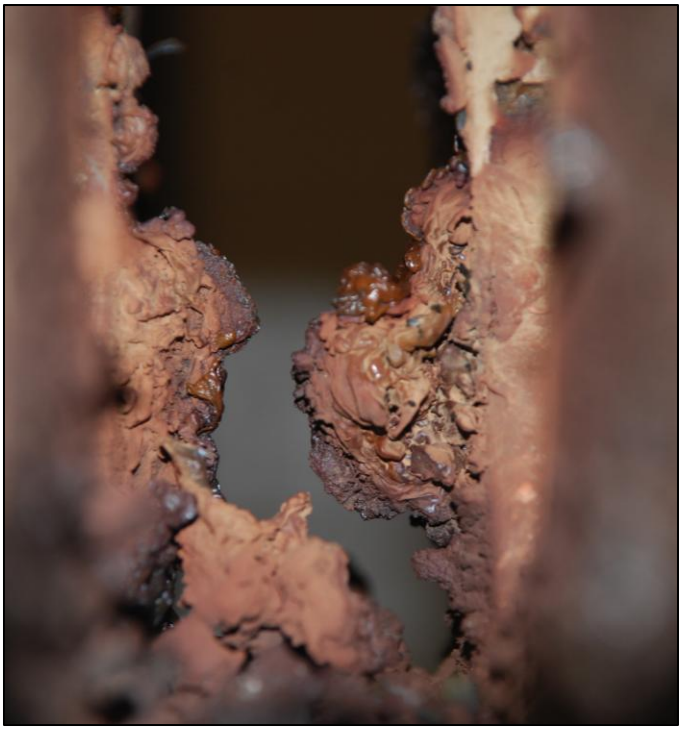

Figure 5.25. Image of deposit structure on transition piece after removal from aerothermal test section.

Figure 5.26. View of the exit of the aerothermal test section.

CHAPTER 6:
Conclusions and Future Work Recommendations

6.1 Summary

The purpose of this study was to examine the evolution of particulate deposition on a pressure surface of a simulated integrated gasification combined cycle (IGCC) film-cooled turbine vane in a high pressure and temperature facility. The high-pressure combustion facility at the National Energy Technology Laboratory (NETL) was used to perform experiments examining the effects of five factors (freestream temperature, impaction angle, blowing ratio, particulate loading, and surface coating process) on particulate deposition growth.

The results of the freestream temperature experiment showed that as the freestream temperature increased the amount of deposition also increased. This finding corresponded with previous studies. Experiments that were performed with temperatures below 2200^{o}F did not accumulate any particulate deposition. The effect of freestream temperature conclusion for this study was that as the temperature increased from 2200^{o}F to 2315^{o}F the deposition would increase.

The impaction angle results also corresponded well with previous studies showing that as the impaction angle increased from 10^{o} to 20^{o} the amount of deposition increased. Two different blowing ratios (M=1.0 and 0.25) were tested for the effects of impaction angle on deposition. The 20^{o} test article had more deposition in both cases when compared to the 10^{o} counterpart. The conclusion of this study was that in the range of 10^{o} and 20^{o} impaction angles the particulate deposition would increase as the impaction angle increased.

The blowing ratio or ratio of mass flux of the coolant to the mass flux of the mainstream flow experiment was performed for three different values: M=0.0, 0.25, and 1.0. As the blowing

ratio increased the amount of deposition decreased. The deposits started blocking the cooling holes due to the lack of flow exiting the holes. The conclusion of this study about blowing ratio is that for blowing ratios between M=0.0 and M=1.0 the particulate deposition will decrease due to lower surface temperature and the jets deflecting particles away.

The particulate loading was varied from 100 ppmw-hr to 200 ppmw-hr by doubling the experiment run time to study the effects it had on particulate deposition. Even with double the run time no new deposits formed across the length of the test article. Instead, significantly more deposits formed on the area that already contained deposits. These results lead to the conclusions that the deposition continually increased and formed a larger structure during a test with twice the particulate loading and that with twice the operational time the film cooling prevented deposit growth downstream of the holes.

The surface coating effect on deposition was examined between the bare metal and thermal barrier coating (TBC) surface. The bare metal surface had considerably less deposition compared to the TBC surface. This result corresponded with previous studies on the subject that describe the roughness of the TBC and low conductivity as reasons for the ability of deposits to form. The conclusion was that between the TBC in this study and the bare metal the particulate matter would deposit more on the TBC coating.

The effects of the swirl attributed to results of this study had an extremely detrimental effect on the deposition of the test articles. The swirl in an actual gas turbine would be washed out before it reached the first stage vanes by dilution cooling. Also, the flow would be channeled into the first stage which would reduce the swirl as well. Therefore, the swirl that was apparent in this study is not an accurate simulation of an actual gas turbine flow field. As particles

approached the test article they were interacting with a cooler boundary layer across the water cooled test article holder. Therefore the swirl would angle the particles in a manner that allowed the formation of deposit structures to only occur on the side that the swirl impacted first. The particles that traveled farther distances across the cooled holder would drop below the sticking temperature and not stick to the test article face. Another reason that deposition formed more regularly on one side of the test article was due to the side obstructing the flow at a 90^{o} angle and creating an impingement. Once deposits started forming on the side the particles would adhere to each other and enlarge the deposit structures on that side of the test article.

Another significant discovery during testing was the thermal barrier coatings overall resistance to deposition sticking to the face. Deposition would form on the test articles during the hot run but once the cool down began the particulate matter would begin to sluff off. This was a departure from numerous studies that could maintain the large structures after cool down. Most studies would display some sluff off during removal but would still have a base layer of structures to be analyzed for roughness characteristics. The 7% Yttrium Stabilized Zirconia (7YSZ) used as the thermal barrier coating layer appeared to resist the permanent attachment of the flyash. In contrast to this the surrounding walls in and downstream of the test section showed large deposit structure growths. These growths were extremely hard and could not be easily removed following the run.

6.2 Recommendations for Future work

Further study is needed in these areas using the high pressure high temperature facility. A facility modification to mitigate the swirl would significantly improve the facility's ability to simulate the pressure side of the vane and perform film cooling work. The large swirl that exits

the combustor should be mitigated in some fashion. This would be costly but would greatly improve the flow conditions going through the channel. Altering the test section to perform tests on actual component geometries would be an improvement.

A preliminary concept developed by Florida Turbine Technologies, Inc. to change the test section setup to accommodate actual turbine hardware can be seen in Appendix C. The facility was designed to be operated at 10 atm but currently was not capable of performing tests at those pressures. Working out the issues with this problem would allow work to be performed at higher pressures that are closer to operating pressure in actual industrial gas turbines. Another suggestion would be to perform an LDV test or another method to calculate the turbulence intensity in the test section. Numerous books (*Gas Turbine Heat Transfer and Cooling Technology* [35]as an example) and papers ([7] as an example) have documented the effects of turbulence intensity on heat transfer and film cooling. Many studies such as [12] use a turbulence grid to set the turbulence level in the test section. It would be interesting to compare the results of this test to other studies with similar (and different) turbulence intensities.

Future work should also include examining the effects on heat transfer once a reliable surface temperature system is completed. Materials analysis will be performed on the test articles. First to look at the surface with a very high resolution scanner and then followed by destructive testing to look at the interaction between the deposition and the TBC. An analysis of the deposition that formed on the test section walls around the test article will be performed also to compare with deposition on the test article.

Overall more experiments are needed to further validate the findings already reported. The facility was down for long periods of time during the study and only a limited amount of

testing time was permitted out of the total test plan when the facility was working again. Future tests examining more time intervals to better understand the effects and growth of deposition would be beneficial. More test article face geometries might shed light on the effects of the impaction angle on the evolution of deposit structures. Looking at the effects of hole spacing would improve the understanding of how deposits form near holes that are spaced close together and far apart. Novel film cooling geometries such as the anti-vortex or sister hole concept would further the work being performed by other graduate students at WVU working on a computational study on the concept.

Finally, getting an accurate system put in place to measure the surface temperature of the test articles during the runs is paramount to creating a legitimate aerothermal facility. Engineers at NETL are working on multiple concepts to narrow down the surface temperature readings. Wireless sensors are being investigated that could monitor the surface temperature in-situ. These suggestions demonstrate the opportunity that is present for a vibrant future working relationship between NETL and WVU to examine areas of need in the gas turbine heat transfer area.

REFERENCES

[1] Solar Turbines, Inc. , "Gas Turbine Overview," 2011. [Online]. Available: http://mysolar.cat.com/cda/layout?m=35442&x=7. [Accessed 9 April 2012].

[2] D. G. Bogard, "Airfoil Film Cooling," [Online]. Available: http://www.netl.doe.gov/technologies/coalpower/turbines/refshelf/handbook/4.2.2.1.pdf. [Accessed 9 April 2012].

[3] A. Hamed, W. Tabakoff and R. Wenglarz, "Erosion and Deposition in Turbomachinery," *Journal of Propulsion and Power,* vol. 22, no. 2, pp. 350-360, 2006.

[4] R. Logan, G. Richards, C. Meyer and R. Anderson, "A Study of Techniques for Reducing Ash Deposition in Coal-Fired Gas Turbines," *Progress in Energy and Combustion Science,* vol. 16, no. 4, pp. 221-233, 1990.

[5] M. P. Boyce, Gas Turbine Engineering Handbook, Burlington: Gulf Professional Publishing, 2006.

[6] J. Bons, J. Crosby, J. Wammack, B. Bentley and T. Fletcher, "High-Pressure Turbine Deposition in Land-Based Gas Turbines from Various Synfuels," *Journal of Engineering for Gas Turbines and Power,* vol. 129, pp. 135-143, 2007.

[7] D. Bogard and K. Thole, "Gas Turbine Film Cooling," *Journal of Propulsion and Power,* vol. 22, no. 2, pp. 249-270, 2006.

[8] G. Richards, R. Logan, C. Meyer and R. Anderson, "Ash Depositoin at Coal-Fired Gas Turbine Conditions," *Journal of Energy for Gas Turbines and Power,* vol. 114, pp. 132-138, 1992.

[9] J. Bons, R. Taylor, S. McClain and R. Rivir, "The Many Faces of Turbine Surface Roughness," *Journal of Turbomachinery,* vol. 123, pp. 739-748, 2001.

[10] J. Jensen, S. Squire, J. Bons and T. Fletcher, "Simulated Land Based Turbine Deposits Generated in an Accelerated Deposition Facility," *Journal of Turbomachinery,* vol. 127, pp. 462-470, 2005.

[11] C. Smith, B. Barker, C. Clum and J. Bons, "Deposition in a Turbine Cascade with Combusting Flow," in *ASME Turbo Expo 2010: Power for Land, Sea and Air,* Glasgow, 2010.

[12] S. a. T. K. Lawson, "Effects of SImulated Particle Deposition on Film Cooling," *Journal of*

Turbomachinery, vol. 133, p. 021009 (9 pages), 2011.

[13] J. Albert and D. Bogard, "Experimental Simulation of Contaminant Deposition on a Film Cooled Turbine Vane Pressure Side With a Trench," in *ASME Turbo Expo 2011: Power for Land, Sea and Air*, Vancouver, 2011.

[14] J. Crosby, S. Lewis, J. Bons, W. Ai and T. Fletcher, "Effects of Particle Size, Gas Temperature, and Metal Temperature on High Pressure Turbine Deposition in Land Based Gas Turbines from Various Synfuels," in *ASME Turbo Expo 2007: Power for Land, Sea and Air*, Montreal, Canada, 2007.

[15] W. Ai, N. Murray, T. Fletcher, S. Harding, S. Lewis and J. Bons, "Deposition Near Film Cooling Holes on a High Pressure Turbine Vane," *Journal of Engineering for Gas Turbines and Power*, vol. 134, 2012.

[16] W. Ai, N. Murray, T. Fletcher, S. Harding and J. Bons, "Effect of Hole Spacing on Deposition of Fine Coal Flyash Near Film Cooling Holes," *Journal of Turbomachinery,* vol. 134, no. 4, p. 041021 (9 pages), 2012.

[17] J. Wammack and J. F. D. B. J. F. T. Crosby, "Evolution of Surface Deposits on a High-Pressure Turbine Blade-Part I: Physical Characteristics," *Journal of Turbomachinery*, vol. 130, pp. 1-8, 2008.

[18] W. Ai, R. Laycock, D. Rappleye, T. Fletcher and J. Bons, "Effect of Particle Size and Trench Configuration on Deposition from Fine Coal Flyash Near Film Cooling Holes," in *ASME Turbo Expo 2009: Power for Land, Sea and Air*, Orlando, Florida, USA, 2009.

[19] R. Laycock and T. Fletcher, "Time-Dependent Deposition Characteristics of Fine Coal Flyash ina Laboratory Gas Turbine Environment," in *ASME Turbo Expo 2011: Power for Land, Sea and Air*, Vancouver, Canada, 2011.

[20] J. Webb, B. Casaday, B. Barker, J. G. A. Bons and N. Padture, "Coal-Ash Deposition on Nozzle Guide Vanes: Part I - Experimental Characteristics of Four Coal Ash Types," in *ASME Turbo Expo 2011: Power for Land, Sea and Air*, Vancouver, Canada, 2011.

[21] E. Erickson, F. Ames and J. Bons, "Effects of a Realistically Rough Surface on Vane Heat Transfer Including the Influence of Turbulence Condition and Reynolds Number," *Journal of Turbomachinery*, vol. 134, no. 2, p. 021013 (8 pages), 2012.

[22] S. Lewis, B. Barker, J. Bons, W. Ai and T. Fletcher, "Effects of Obstructions and Surface Roughness on Film Cooling Effectivenesss with and Without a Transfer," *Journal of*

Turbomachinery, vol. 133, no. 3, p. 031003 (9 pages), 2011.

[23] R. Murphy, A. Nix, S. Lawson, D. Straub and S. Beer, "Preliminary Experimental Investigation of the Effects of Particulate Deposition on IGCC Turbine Film Cooling in a High-Pressure Combustion Facility," in *ASME Turbo Expo 2012: Power for Land, Sea and Air*, Copenhagen, Denmark, 2012.

[24] G. Energy, Interviewee, *Technical conversation about pressure surface Reynolds numbers of large industrial gas turbine.*. [Interview]. 3 March 2011.

[25] I. Directed Vapor Technologies International, "Directed Vapor Technologies International, Inc.," 2011. [Online]. Available: www.directedvapor.com. [Accessed 20 March 2012].

[26] SCITEK Consultants Ltd., "Powder Seeders," Scitek Consultants, [Online]. Available: http://www.scitekconsultants.co.uk/7/Powder-Seeders. [Accessed 14 October 2011].

[27] J. Bons, J. Wammack, J. Crosby, D. Fletcher and T. Fletcher, "Evolution of Surface Deposits on a High Pressure Turbine Blade, Part II: Convective Heat Transfer," in *ASME Turbo Expo 2006: Power for Land, Sea and Air*, Barcelona, Spain, 2006.

[28] Intertek, "LS Particle Size Analyzer," Chicago, Illinois, 2010.

[29] C. Crowe, Multiphase Flow Handbook, CRC Press, Taylor and Francis Group, 2009.

[30] R. Dennis, W. Shelton and P. Le, "Development of Baseline Performance Values for Turbines in Existing IGCC Applications," in *ASME Turbo Expo 2007: Power for Land, Sea and Air*, Montreal, Canada, 2007.

[31] D. Hautman, R. Haas and L. Chiappetta, "Transverse Gaseous Injection Into Subsonic AIr Flows," in *29th Aerospace Sciences Meeting*, Reno, NV, 1991.

[32] F. Incropera, D. Dewitt, T. Bergman and A. Lavine, Introduction to Heat Transfer, John Wiley and Sons, Inc., 2007.

[33] S. Lawson, Interviewee, *Personal Communication Concerning Future IR Measurement Systems for High Pressure Facility.* [Interview]. 29 March 2012.

[34] D. E. Sabolsky, Interviewee, *Discussions about fly ash and high silica based refractory interactions.*. [Interview]. 19 April 2012.

[35] J. Han, S. Dutta and S. Ekkad, Gas Turbine Heat Transfer and Cooling Technology, Taylor & Francis, 2000.

APPENDIX A:
MathCAD Formulas

Injection Tube Parameters

$d_{tube} = 0.152 \text{ in}$

$A_{tube} = \frac{\pi}{4}(d_{tube})^2$

Combustor Tube Parameters

$d_{comb} = 4 \text{ in}$

$A_{comb} = \frac{\pi}{4}(d_{comb})^2$

Equation of State:

$R_{gas} = 8.314 \frac{J}{mol * K}$

$\rho(p, T, MW) = \frac{p * MW}{R_{gas} * T}$

Facility Parameters

$p_{rig} = 8\ atm$

$T_{rig} = 1366.483\ K$

$Q_{SCFH} = 68588\ \frac{ft^3}{s}$

$\rho_{rig} = \rho\left(p_{rig}, T_{rig,} 0.028 \frac{kg}{mol}\right) = 1.998 \frac{kg}{m^3}$

Nitrogen Parameters

$T_{N2} = 300\ K$

$Vel_{N2} = 200\ \frac{ft}{s}$

$$MW_{N2} = 28.0\ \frac{gm}{mol}$$

$$\rho_{N2} = \rho\left(p_{rig}, T_{N2,} MW_{N2}\right) = 9.1 \frac{kg}{m^3}$$

Mass Flow Rates

$$m_{N2} = \rho_{N2} * A_{tube} * Vel_{N2} = 6.494x\ 10^{-3} \frac{kg}{s}$$

$$m_{rig} = \rho\left(14.7psi, 520R, 28.97 \frac{gm}{mol}\right) * Q_{SCFH} = 0.66 \frac{kg}{s}$$

Velocity and Momentum Ratio

$$V_{rig} = \frac{m_{rig}}{\rho_{rig} * A_{comb}} = 40.72 \frac{m}{s}$$

$$MR = \frac{\rho_{N2} * (Vel_{N2}^2)}{\rho_{rig} * \left(Vel_{rig}^2\right)} = 10.208$$

Injection Depths

$$Y_{min}(Z) = 0.31 * d_{tube} * MR^{0.5} \left(\frac{Z}{d_{tube}}\right)^{0.33}$$

$$Y_{mid}(Z) = 0.56 * d_{tube} * MR^{0.5} \left(\frac{Z}{d_{tube}}\right)^{0.33}$$

$$Y_{max}(Z) = 0.73 * d_{tube} * MR^{0.5} \left(\frac{Z}{d_{tube}}\right)^{0.33}$$

APPENDIX B:
Raw Roughness Results

Table A.1. Raw Roughness Results for 3-Hour Run

Parameter	Description	Height (μm)
SRp	Maximum Peak Height	738
SRv	Maximum Valley Depth	467
SRz	Avg Maximum Height	1205
Sra	Roughness Average	51
SRq	Root Mean Square Avg	88

Table A.2. Raw Roughness Results for 6-Hour Run

Parameter	Description	Height (μm)
SRp	Maximum Peak Height	1198
SRv	Maximum Valley Depth	1100
SRz	Avg Maximum Height	2298
Sra	Roughness Average	237
SRq	Root Mean Square Avg	299

APPENDIX C:
Proposed Test Section Redesign

The image below shows the proposed test section redesign by Florida Turbine Technologies, Inc. The new test section would allow novel film cooling hole geometries to be tested on a surface that had the same geometric conditions of an actual turbine vane/blade. Optical access would be available on the pressure side of the test article. The flow field would be representative of the flow field around an actual gas turbine vane. This new design would not be conducive to deposition studies due to the high Stokes numbers leading to wall impaction at the turn.

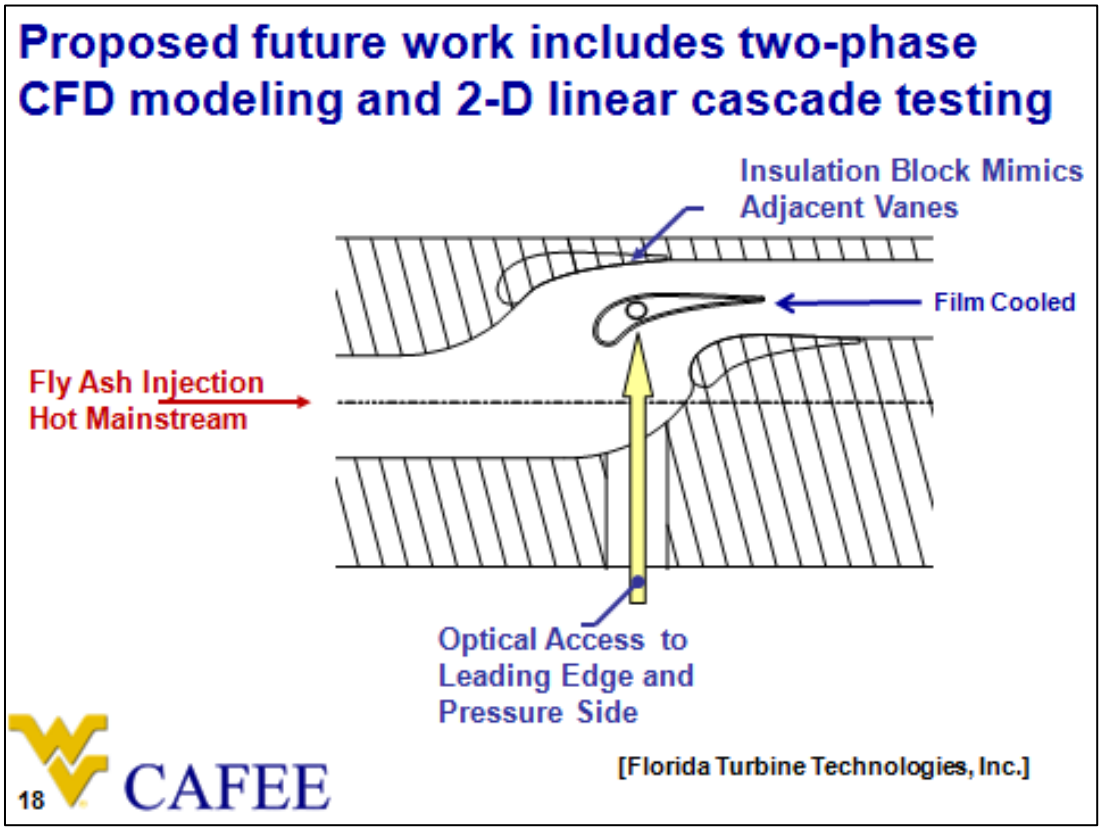

APPENDIX D:
ASME Turbo Expo 2012 Conference Paper

The following pages are part of a conference paper that was presented at the American Society of Mechanical Engineers (ASME) Turbo Expo 2012: Power for Land, Sea and Air in Copenhagen, Denmark. The paper discusses the preliminary work of this study. An abstract submission is anticipated detailing the final results of this study to be presented at ASME Turbo Expo 2013: Power for Land, Sea and Air in San Antonio, Texas.

Proceedings of ASME Turbo Expo 2012: Power for Land, Sea and Air
GT2012
June 11-15, 2012, Copenhagen, Denmark

GT2012-68806

PRELIMINARY EXPERIMENTAL INVESTIGATION OF THE EFFECTS OF PARTICULATE DEPOSITION ON IGCC TURBINE FILM-COOLING IN A HIGH-PRESSURE COMBUSTION FACILITY

Robert G. Murphy, Andrew C. Nix and Seth A. Lawson
Center for Alternative Fuels, Engines and Emissions
Department of Mechanical and Aerospace Engineering
West Virginia University
Morgantown, WV, USA

Douglas Straub and Stephen K. Beer
National Energy Technology Laboratory
U.S. Department of Energy
Morgantown, WV, USA

ABSTRACT

Researchers at West Virginia University are working with the U.S. Department of Energy, National Energy Technology Laboratory (NETL) to study the effects of particulate deposition on turbine film cooling in a high pressure and high temperature environment. To simulate deposition on the pressure side of an Integrated Gasification Combined Cycle (IGCC) turbine first stage vane, angled film-cooled test articles with thermal barrier coatings (TBC) are subjected to accelerated deposition at a pressure of approximately 4 atm and a gas temperature of 1100^{o}C. Two different test article geometries were designed, with angles of 10^{o} and 20^{o} to the mainstream flow. Both geometries have straight-cooling holes oriented at a 30^{o} angle to the hot-side surface. A high pressure seeding system was used to generate a particulate concentration of approximately 33.3 ppmw. Particle concentrations of 0.02 ppmw exist in the IGCC hot gas path. An accelerated simulation method was developed to simulate deposition that would occur in 10000 hr of engine operation. Preliminary tests were performed at 4 atm and 1100 ^{o}C to validate the deposition process. The results showed more deposition on the 20^{o} test article than the 10^{o} test articles; however no substantial deposition developed on either test article. A lumped mass analysis showed that the fly ash particles dropped below the theoretical sticking temperature as they approached the test article. Deposition was analyzed non-destructively through visual observation and scanning with a scanning laser microscope. Based on the initial test run results, a detailed plan was created to increase the operating temperature of the rig and allow two 3-hour tests to be performed on each of the test articles. Non-destructive testing will be used before, in between and after the runs to examine the evolution of the deposition growth. Following the final run, destructive testing will be used to examine the chemical composition of the deposits and their potential interaction with the TBC. Preliminary work will lead to a future study the would enhance the understanding of particle deposition evolution and examine the effects of deposition on film cooling by performing the tests in a high-pressure and high-temperature environment that is similar to the high-pressure combustion exhaust gas environment of the first stage region in IGCC turbines.

INTRODUCTION

The need to understand the development of particulate deposition is important to increase the life of the hot stage components in an Integrated Gasification Combined Cycle (IGCC) gas turbine. Deposition can have a devastating effect to the film-cooling scheme by altering cooling patterns both upstream and downstream of the cooling holes, and potentially block film cooling holes. Deposits in the turbine section are a product of impurities in inlet air or fuel from upstream combustion that, upon entering the turbine section, deposit on the components in the flowpath [1]. In recent years more emphasis has been placed on understanding the evolution of particulate deposition, its effects on thermal barrier coatings (TBC) and the effects it has on heat transfer.

An understanding of the mechanisms of deposition is important to accurately simulate deposits in a combusting flow. Hamed et al. [1] listed the four mechanisms of particle delivery as inertial impaction, turbulent diffusion/eddy impaction, Brownian diffusion and thermophoresis. Richards et al. [2] described three mechanisms of the deposition process being particle adhesion, deposit erosion and deposit spallation. The facility used in the study by Richards et al. [2] was a high-temperature facility at 1 atm pressure. The flow would impinge on a backside cooled flat test article where the fly ash would be deposited. They concluded that as the surface temperature of the test article increased the ability of the particulate matter to "stick" to the surface increased.

Understanding roughness characteristics is important to the process of modeling it. Bons et al. [3] examined almost

100 land-based turbine components and analyzed them to create 3D surface maps of the surface roughness. This work showed the evolution of degradation in the blades from pitting, to craters and finally exposed metal. The deposits near film cooling holes were found to increase at the point where cooling air was injected and also downstream of the holes.

Once an understanding of the mechanisms and microstructure of the deposition was reached, facilities were built to simulate long-term deposition in a manageable laboratory experiment. Several groups developed facilities to accelerate deposition such as Jensen et al. [4], Smith et al. [5], and Lawson and Thole [6]. At BYU Jensen et al. [4] developed the Turbine Accelerated Deposition Facility (TADF) to simulate 10,000 operating hours in a 4-hour test by depositing material onto a flat test article. The facility matches the Mach number and flow temperature of the first stage high-pressure turbine blades but does not match the pressure. Jensen et al. [4] concluded that the surface topography, microstructure and chemical composition found in the accelerated deposition process resembled actual industrial gas turbine deposition. Smith et al. [5] developed the Turbine Reacting Flow Rig (TuRFR) to simulate deposition on nozzle guide vanes in combusting flow during a 1-2 hour test. Coal ash was injected into the flow at high particulate loadings to simulate the particulate deposition of several thousand hours of run time. The test article consisted of two nozzle guide vane (NGV) doublets. The TuRFR facility was capable of matching the pressure and inlet Mach number of an industrial gas turbine but not at elevated pressures. The conclusions from this work showed that this method of accelerated deposition was sufficient for simulating roughness characteristics caused by deposition on actual engine hardware. The study concluded that film cooling reduced the evolution of surface deposits. Lawson and Thole [6] used a low speed wind tunnel with low melt wax to simulate particle deposition. Non-dimensional Stokes similarity was used to scale the inertial characteristics of fly ash particles in engine conditions by using larger wax particles in laboratory conditions. A large-scale open loop test channel was used to determine the effects of deposition on a film cooled flat plate at conditions close to standard temperature and pressure. Lawson and Thole [6] found that deposition decreased with an increase in coolant mass flow because coolant jets diverted particle trajectories and cooled particles preventing them from sticking upon impacting the surface. Albert and Bogard [7] performed experiments in a facility similar to one used by Lawson and Thole [6]. The main difference was that the wax was being deposited onto a large-scale 2-passage vane cascade. The work examined an isothermal vane and an internally cooled vane. The results showed that the surface temperature plays an important role in deposition. The isothermal blade had significant deposition along the pressure side while the internally cooled blade had very little in the same area.

Wammack et al. [8] used the TADF to study the evolution of deposits over the course of 10000 simulated operating hours. The particulate concentration was scaled up so that the tests could be run in a matter of hours. The results showed that there was an initial buildup of deposition with peaks and valleys followed by a period where the valleys would be filled in. After the valleys were filled in more deposition with peaks and valleys would form on top of it. Crosby et al. [9] studied the effects of particle size, gas temperature and metal temperature on deposition. The study showed that as the mean particle diameter increased from 3 to 16 μm the deposition rate more than doubled. When the gas temperature was reduced, the rate of deposition decreased. At temperatures below 960 ^{o}C no deposition was observed. Webb et al. [10] used the TuRFR to examine the effects that different compositions of fly ash would have on the ability of the fly ash to deposit onto the components. They found that the mainstream temperature needed to reach between 1044-1060 ^{o}C depending on the composition of the fly ash to soften the particles enough to cause deposition.

Understanding the evolution of deposition on turbine components in realistic engine conditions is critical to reducing the downtime of industrial gas turbines. The previous work in this field has produced valuable results on the effects of gas temperature, particle sizing and surface temperature at elevated temperatures. However, none of these studies have simulated the high pressures that exist in an actual gas turbine. The current study describes the methods developed to simulate accelerated deposition in a gas turbine engine at elevated pressures and temperatures by modifying an existing gas turbine combustion facility by installing an aerothermal test section and a system to inject coal fly ash into the facility downstream of the combustor.

EXPERIMENTAL METHODS

The following sections describe the high-pressure combustion facility and particulate deposition simulation methods that were developed for this preliminary investigation. The methods described in this section will be used to conduct a more comprehensive study on the effects of particulate deposition on film cooling at high pressure operating conditions.

High Pressure Combustion Facility

Preliminary deposition experiments were conducted in the National Energy Technology Laboratory (NETL) Aerothermal Test Facility, which consists of a high-pressure gas turbine combustion research rig that was modified to conduct turbine-related aerothermal and heat transfer research. For the current study, the hot gas path was pressurized to 4 atm. Pressurized air for combustion and cooling was supplied to the test rig through six independent flow loops at a maximum combined flow rate of 0.9 kg/sec. Natural gas was used as the fuel, and was supplied to the test rig through two independent flow loops at a maximum combined flow rate of 12 g/sec.

A combustor was located upstream of the aerothermal test section to provide a swirling, turbulent, high temperature flow to the test section for heat transfer studies. The combustor design was a swirl-stabilized, lean premixed combustor. The premix nozzle was an annulus with a 63.5 mm outer diameter, surrounding a 38.1 mm diameter cylindrical centerbody that extended along the centerline axis of the premixer. Pilot fuel was injected through an array of

fuel was injected axially and radially into the premix fuel-air stream. The air and fuel from the premix nozzle fed into the combustion region, which was bounded by a fused silica tube liner with a 180 mm inner diameter and 300 mm length. The fused silica combustor liner allowed for optical access to the entire length of the combustion region through an array of viewports surrounding the pressure vessel. Immediately downstream of the combustion region, the flow area reduced to a nominal 105 mm diameter combustor exhaust duct with water-cooled walls. It is important to note that the water used for cooling did not mix with the hot process gas and no dilution jets or other film cooling was used upstream of the aerothermal test section. An isometric view of the high-pressure combustion rig is shown in Figure 1.

Between the cooled combustor exhaust duct and the aerothermal test section was another flow area transition, which converted the dimension and shape of the flow path from a round to a rectangular flow area. The cross-sectional area transitioned from a nominal 105 mm diameter to a rectangular (51 mm wide x 127 mm high) cross-section. The transition was constructed using a cast high-density zirconia refractory, and the walls of the rectangular flow path were constructed using a conventional high-alumina, dense-castable refractory. This dense-castable refractory wall was surrounded by an insulating refractory layer that protected the pressure vessel from the hot gas path.

The pressure vessel for this test section was constructed using carbon steel components. Three 10 cm studding outlets were oriented 90° apart around the circumference of the 46 cm diameter carbon steel vessel. One of the 10 cm ports was used to install the test article. The port that was oriented 90° from the other two ports was used to monitor the gas temperature using a conventional (Type-K) thermocouple. An image of the cross-section of the high-pressure combustor and test section is shown in Figure 2.

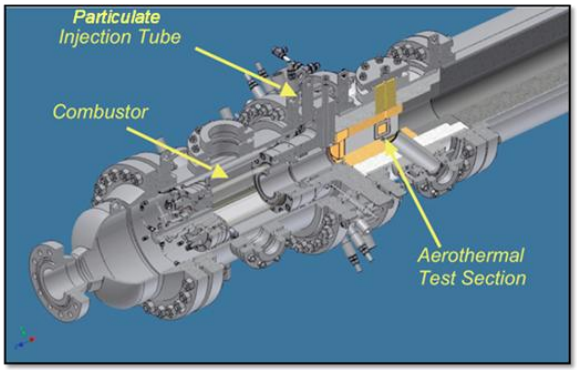

Figure 1. Isometric view of the high pressure combustor and downstream aerothermal test section at NETL.

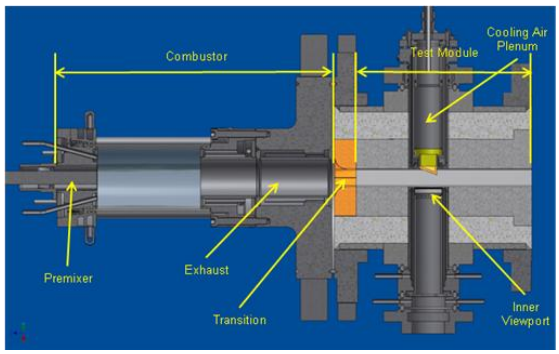

Figure 2: Cross-section of the high pressure combustor and downstream aerothermal test section at NETL.

For this study, all of the test samples were constructed out of Haynes 230 material. Each test sample was installed into a fixture that mechanically compressed the sample into place. The insertion depth of the test fixture was adjustable to allow the test sample to be positioned flush with the vertical refractory walls. Conduction losses to the fixture were reduced, but not eliminated, using a ceramic gasket material between the test sample and the test fixture.

Cooling air for the test sample entered the cooling air plenum through a 12.7 mm diameter tube. For the data described in this paper, the cooling air entered the test fixture at room temperature. The cooling air stream flowed through approximately 326 mm of a 67 mm diameter plenum before being injected as film cooling air through the test sample. All of the cooling air that was injected into the plenum flowed through the test article film cooling holes. A thermocouple (Type-K) was placed in the cooling air plenum approximately 25 mm away from the test sample. The estimated bias of this measurement is expected to be 5 to 10K.

The surface temperature on the plenum side of the test sample was measured using two Type-K thermocouples. One thermocouple was located on the cold side between the exits of two cooling holes. The second thermocouple was located on the cold side at the downstream edge of a cooling hole exit. The Type-K thermocouples routed through a 0.8 mm diameter Inconel sheath were held to the surface by welding stainless steel foil strips to the back of the test specimen. The thermocouple beads were attached to the test article backside surface using high thermal conductivity Cotronics 906 Magnesia Adhesive (k = 5.8 Wm-K) to improve the thermal contact.

The surface temperature on the hot-gas side of the test sample was monitored using a single-wavelength infrared (IR) imaging technique. The primary advantage of this approach was that it did not require direct contact with the surface, so it was less intrusive than other approaches. The disadvantage of this approach was the significant uncertainty that was introduced by reflections from the surrounding hot walls and potential variations in the surface emissivity, or reflectivity, that can be caused by surface oxidation at high temperature. The preliminary data presented in this paper does not include

these surface temperature measurements; however, the design of the viewport assembly is described for completeness.

The viewport assembly was installed in the opposite wall of the test section hot gas flow path. Two windows were mounted in the optical viewport assembly. The first (interior) window was situated flush with the interior wall to provide a smooth flow transition across the viewport opening. This interior window was a 76.2 mm diameter x 12.7 mm thick fused silica disk that was supported in a viewport fixture. A cooling air purge was introduced through a 0.6 mm slot along the leading edge of the window. After providing film cooling for the viewport, this purge flow mixed with the hot process gas downstream of the viewport. At temperatures above 1000°C, fused silica can experience a phase change (devitrification) that results in a significant optical transmission loss. The cooling air purge was an attempt to reduce de-vitrification of the interior fused silica window. The second (exterior) window was a commercial sightglass, which was mounted to the outside of the pressure vessel and acted as a pressure boundary. The IR transmission properties for the fused silica were measured and typically exceeded 90% transmission below 2.3 μm.

Test Article Design

Two test articles having incline angles of 10^o and 20^o were designed to simulate the pressure side of a first stage turbine vane. The backside of both test articles was hollowed out to supply backside cooling evenly to the face. Four cylindrical cooling holes with ~3.9 mm diameter were located on the front side of the face. The pitch of the cooling holes was 2d. Reynolds similarity was used to scale the free stream conditions at the first stage vane row of a large industrial gas turbine to the combustion facility at NETL. This results in a scaling factor of 8X, applied to the cooling hole diameter, to a real industrial gas turbine vane. Figure 3 displays the drawings of the test articles.

Thermal Barrier Coatings (TBC) were applied to the test articles by Directed Vapor Technologies International (DVTI) using the directed vapor deposition (DVD) process.

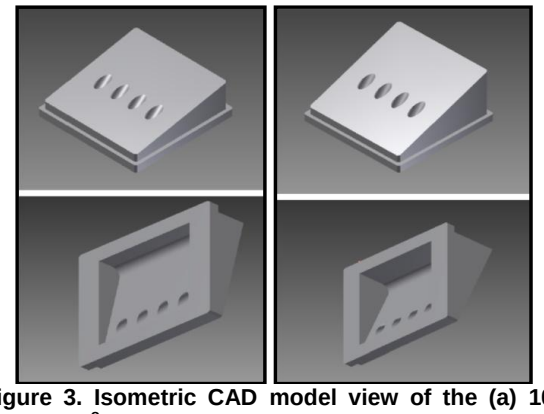

Figure 3. Isometric CAD model view of the (a) 10^o and (b) 20^o test articles.

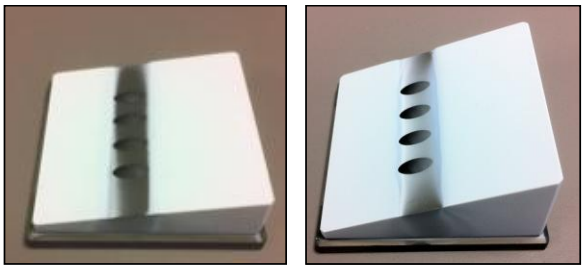

(a) (b)

Figure 4. Photographs of the (a) 10^o and (b) 20^o test articles with TBC before deposition testing.

This process is a more efficient coating process similar to electron beam physical vapor deposition (EB-PVD), with an inert gas jet around the vapor to direct it toward the surface. The bond coat was γ–γ' platinum aluminide (PtAl) with an approximate thickness of 15-20 μm. The TBC layer is 7%Yttrium Stabilized Zirconia (7YSZ) with an approximate thickness of 400 μm as measured by an Olympus OLS 3100 Laser Confocal Microscope. A shallow trench was formed during the coating process due to the cooling holes being masked. Photographs of each test article after coating are shown in Figure 4.

Particulate Composition, Scaling and Seeding

A method was developed to process the fly ash that was injected into the high-pressure combustion facility. The fly ash was baked for approximately 45 minutes in a toaster oven to remove any moisture. A flourmill was then used to grind the fly ash. Particles larger than 45 microns were filtered using a shaker table. The composition and sizing analysis of the particulate matter was performed by Intertek in Chicago, Il. The mean particle size of the processed flyash was approximately 13 μm. Table 1 below displays the composition comparison of the bituminous fly ash in the current study to Smith et al. [5].

A comparison was also conducted between the size of the fly ash used in the current study and the fly ash from Smith et al. [5]. Figure 5 displays the comparisons of the size distributions of both processes. The average particle diameter used by Smith et al. [5] was 14 μm, which closely matches the particulate size used in the current study.

A Stokes analysis was performed to compare particle inertial characteristics between engine and laboratory conditions. The Stokes number is a measure of whether particles will follow fluid streamlines, or their own inertial path. Stokes numbers were calculated for fly ash particles ranging from 0.5 μm to 47 μm for the engine and laboratory conditions shown in Table 2. For this analysis, it was assumed that particles were traveling with the same velocity as the mainstream hot gas path. The engine mainstream velocity, U_∞ = 150 m/s, was calculated assuming a turbine inlet Mach number of 0.2 and a turbine inlet temperature of 1509 K [11]. The film-cooling hole diameter was selected as the appropriate obstacle length scale for calculating Stokes number in these experiments.

Table 1: Bituminous Coal Ash Composition

Composition	Smith et al. [5]	WVU
SiO_2	32.9	53.8
CaO	2.93	4.39
Fe_2O_3	40.6	8.87
Al_2O_3	20.3	25.35
SO_3	0.827	1.15
K_2O	2.48	2.23

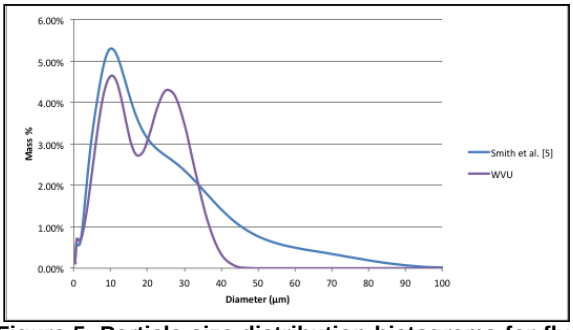

Figure 5. Particle size distribution histograms for fly ash at different processing stages.

Table 2. Stokes Number Conditions

	Laboratory	Engine
Mainstream Temperature, T_∞ (K)	1339	1509 [11]
Fly Ash Density [12], ρ_p (kg/m^3)	1980	1980
Cooling Hole Diameter, d (mm)	4.0	0.5
Mainstream Velocity, U_∞ (m/s)	66	150
Mainstream Viscosity, µ	4.9×10^{-5}	5.3×10^{-5}
Median Particle Size, $d_{p,med}$ (µm)	13.0	3.2
Median Particle Stokes Number, Stk_{med}	6.3	6.3

Figure 6 shows the Stokes number distribution with respect to fly ash particle diameter for engine and laboratory conditions. The reference lines in Figure 6 show that 13 µm particles in the laboratory had the same Stokes number as 3.2 µm particles in the engine. Although the exact distribution of particle sizes that exist in actual engine conditions is unknown, all particles greater than 10 µm and most particles greater than 1 µm are removed by modern filtration systems [12]. Therefore, it is appropriate to assume that the median fly ash particle size that exists in engine conditions is on the order of 3 µm. The Stokes analysis presented here shows that particle inertial characteristics can be matched between engine and laboratory conditions.

A PS-20 Scitek particle seeder shown in Figure 7 was used to inject the fly ash particulate into the combustion rig. The seeder was capable of being pressurized up to 20 atm to allow particulate injection into high pressure environments and was designed specifically to ensure particles were entrained into the flow with minimal agglomeration.

Several issues arose with the installation of the seeder. The pressure drop across the seeder was very low with the initial setup. It was determined that the length of the tubing was too long and it was creating a large pressure loss before it entered the rig. The total tubing length from the seeder to the combustion was reduced to stop the large pressure loss that occurred in the tubing at a flow rate of 9 g/s. After this correction the seeder was still not injecting enough fly ash so a needle valve was installed just upstream of the seeder to meter

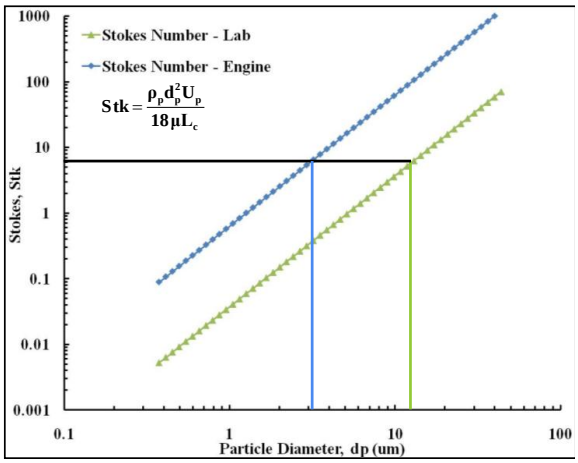

Figure 6. Stokes numbers plotted with respect to particle diameter for fly ash particles in engine and laboratory conditions.

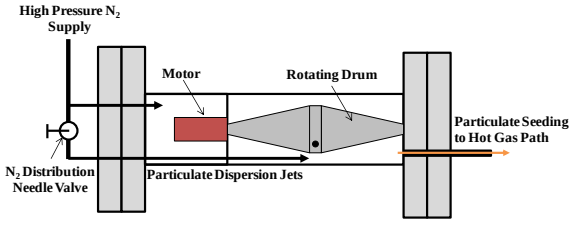

Figure 7. Scitek PS-20 particle seeder used to inject fly ash particles into hot gas path.

the incoming flow and increase the agitation of the fly ash inside the pressure vessel (see Figure 7).

Upon inspection of the interior walls around the injection point it was found that a lot of the particulate matter was impacting the opposing wall to the injection tube. A jet in crossflow analysis showed that at the operating conditions the fly ash would impinge on the opposite wall. A modification to the injection tube was raised approximately 4 cm to create a diffuser effect to lower the outlet velocity and allow the fly ash to be seeded into the center of the test section area.

A lumped mass analysis was performed to determine whether the particles reached thermal equilibrium before impacting the test article. The correlation shown by Equation 1 was used to calculate the heat transfer coefficient for the lumped mass analysis [13].

$$Nu_{d_p} = 2 + 0.6Re_{d_p}^{1/2}Pr^{1/3} \quad (1)$$

Where Nu_{dp} is the Nusselt number, Re_d is the particle Reynolds number based on slip velocity and Pr is the Prandtl number. A worst case scenario no slip condition was used by setting the Re_d to zero which reduced the equation to the Nusselt number having a value of two. The heat transfer coefficient determined from the definition of Nu_D in Equation 1 was used in the lumped mass analysis to calculate the distance required for the particles to reach thermal equilibrium. The analysis showed that greater than 85% based on mass of the particles would be in thermal equilibrium with the hot exhaust gases at a distance of 8.52 cm downstream of the particle injection tube which ensured that particles would be at thermal equilibrium upon reaching the test article. This analysis was performed assuming no swirl in the channel. However, the authors believe that the swirl will only extend the time it takes the particles to reach thermal equilibrium therefore the analysis is valid to prove that the majority of the particles will be at thermal equilibrium.

PRELIMINARY EXPERIMENTAL RESULTS

Preliminary tests were performed using the high-pressure combustion rig. Due to a limitation in the design of the refractory lining, the pressure and temperature were limited to 4 atm and 1400K, respectively for these preliminary tests. The freestream velocity of the combustion rig in the test section was 65 m/s. The blowing ratio of film cooling was 1.0.

Preliminary tests were performed with both the 10^o and 20^o test articles being run for 3 hours at a particle concentration of 33.3 ppmw. The 20^o test articles had visible deposition on the surface while the 10^o test articles did not. These two test articles are shown in Figure 8.

Upon inspection the test section walls showed more deposition than the test article and holder. Neither test article displayed substantial deposition in relation to the test section walls. However, it is interesting to note that the 20^o test article exhibited more deposition than the 10^o as shown in Figure 8. This was most likely caused by the inclination angle being greater on the 20^o test article, which caused the particles to be more ballistic and increase the probability that the particles would impact the face. An image showing the deposition coating the interior walls can be seen below in Figure 9.

After the deposition was found on the walls, another lumped mass analysis was performed to estimate the particle

(a) **(b)**

Figure 8. Photographs of the (a) 10 degree test article and (b) 20 degree test article after 3-hour run at M=1.0.

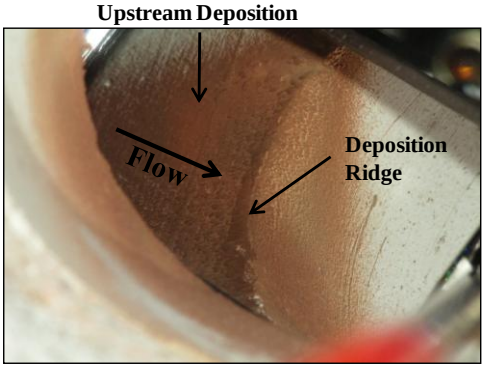

Figure 9. Fly ash deposition upstream of the test article on the interior refractory wall.

temperature as it approached the test article. The thermal analysis showed that as the particles approached the cooled test article the temperature of the particle dropped below the theoretical sticking temperature of 1044^oC [10]. A new refractory liner has been designed to allow the rig to operate at higher pressures and temperatures which will mitigate the problem of the particle temperature dropping below the sticking temperature.

An Olympus LEXT OLS 3100 laser confocal microscope was used to perform a characterization of the surface roughness of the test articles. The microscope was used with a 5 μm resolution. The computer program that accompanies the microscope was capable of filtering out noise and correcting tilts in the scanning field. The microscope was capable of scanning minute contaminations such as the silica contaminations seen in Figure 10. The silica deposits on the TBC on several of the test articles were caused by a contamination during the DVD coating process. The laser microscope was used to take scans before and after the 3-hour test of the 20^o test article. The surface roughness scans can be seen in Figure 11.

As Figure 11 displays, very little deposition was observable by the microscope on the post-deposition article. As illustrated in Figure 8b, a very thin red deposition layer was observed on the 20° test article. As stated above, the lack of deposits on the test article is due to the particles dropping below the sticking temperature as they approach test article.

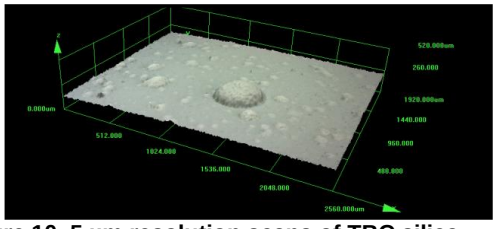

Figure 10. 5 µm resolution scans of TBC silica contamination.

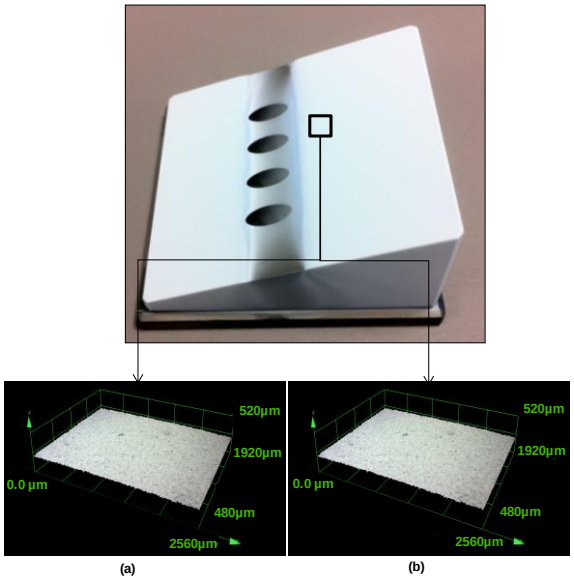

Figure 11. 5 µm resolution scans of the 20° test article (a) before and (b) after the 3-hour run.

FUTURE WORK

A test plan has been developed to operate the combustion rig at higher temperatures with the new refractory. Each test article geometry will be subjected to two 3-hour tests at a particle concentration of 33.3 ppmw to simulate 10,000 operating hours of an industrial gas turbine engine. A black and white thermography camera system, as described earlier, will be used to observe the film cooling patterns during the test. This camera system will allow observation of the film cooling pattern alterations that occur as deposits form on the surface.

The test articles surface roughness has been characterized after the TBC was applied for the baseline measurement using the Olympus LEXT OLS 3100. After the first 3 hour experiment, the test articles will be scanned and characterized again and then for the final time after the second run. The microscope and accompanying program will be used to generate 3-D surface maps of the deposition for the entire test article surface, as compared to the small areas shown in Figure 11. By making microscopic surface measurements at three stages in the evolution of deposition, a better understanding of deposition formation can be obtained. Following the last test, destructive testing will be performed to ascertain the chemical composition of the deposition and their potential interaction with the TBC.

SUMMARY AND CONCLUSIONS

The modifications to the high-pressure combustion facility were completed to allow the facility to be used as a high pressure and temperature deposition and aerothermal test facility. Two test article geometries were manufactured and coated with a TBC. The test article cooling holes were scaled using Reynolds similarity to match the free stream condition of an actual industrial gas turbine first stage vane. A process was developed to bake, grind, and sieve the fly ash to match the particle distribution and composition in the literature as well as match the inertial characteristics using Stokes analysis of the fly ash particles to the inertial characteristics of the particulate matter in an actual industrial gas turbine engine.

The preliminary tests show that the facility was capable of seeding the required fly ash into the test section. The 20° test article had more deposition on the face than the 10° test article, which is believed to be a result of the particles being more ballistic as they approach the 20° test article. However, the majority of the fly ash did not stick to the test articles due to the particles dropping below the theoretical sticking temperature as they approached the lower temperature of the test article and its holder. Plans have been developed to raise the temperature of the combustion rig to keep the particles above the sticking temperature as they impact the test article. A testing plan was developed to examine the evolution of the deposits at higher temperatures. This plan includes two runs of 3 hours with non-destructive surface roughness scanning before, in between and after the runs. Finally, destructive testing will be performed after the final run to examine the chemical composition of the deposition and their potential interaction with the TBC.

ACKNOWLEDGMENTS

The authors would like to acknowledge the support of the Department of Energy, Office of Science, Experimental Program to Stimulate Competitive Research (EPSCoR) under grant/contract number DE-FG02-09ER46615, monitored by Dr. Tim Fitzsimmons. In addition, the project was partially funded by the US Department of Energy, National Energy Technology Laboratory through a cooperative agreement with EPSCoR. Several people deserve acknowledgements for their contributions to this project. The authors would like to thank Dr. Keith Kruger of Haynes, International for donating the Haynes 230 test article material. Dr. Derek Hass and Balvinder Gogia of Directed Vapor Technologies International, Inc. (DVTI) cost shared the thermal barrier coatings that were applied to the test articles. Thanks also to

Dr. Geo Richards, Todd Sidwell, Jeff Riley and Mark Tucker for all of their support provided throughout this project.

NOMENCLATURE

c_p	particle specific heat
d	film cooling hole diameter, d = 3.9 mm
d_p	particle diameter
h	heat transfer coefficient
L_c	cooling hole diameter length scale
L_p	particle travel distance
k	thermal conductivity
M	film cooling blowing ratio, $M = \rho_c U_c / \rho_\infty U_\infty$
Nu	Nusselt number, $Nu = hd_p/k$
Pr	Prandtl Number, $Pr = c_p\mu/k$
Re_d	Reynolds number, $Re_d = \rho U_\infty d/\mu$
Stk	Stokes number, $Stk = \rho_p d_p^2 U_p / 18\mu L_c$
T	temperature
U	velocity

Greek

ρ	density
μ	gas dynamic viscosity

Subscripts

c	coolant
med	median
p	particle
∞	mainstream

REFERENCES

[1] Hamed, A., Tabakoff, W., 2007, "Erosion and Deposition in Turbomachinery," *Journal of Propulsion and Power*, **22** (2), pp. 350-360.

[2] Richards, G.A., Logan, R.G., Meyer, C.T., and Anderson, R.J., 1992, "Ash Deposition at Coal-Fired Gas Turbine Conditions: Surface and Combustion Temperature Effects," *J. of Energy for Gas Turbines and Power*, **114**, pp. 132-138.

[3] Bons, J.P., Taylor, R.P., McClain, S.T., and Rivir, R.B., 2001, "The Many Faces of Turbine Surface Roughness," *Journal of Turbomachinery*, **123**, pp. 739-748.

[4] Jensen, J.W., Squire, S.W., Bons, J.P., and Fletcher, T.H., 2005, "Simulated Land-Based Turbine Deposits Generated in an Accelerated Deposition Facility," *Journal of Turbomachinery*, **127**, pp. 462-470.

[5] Smith, C., Barker, B., Clum, C., and Bons, J., 2010, "Deposition in a Turbine Cascade with Combusting Flow," GT2010-22855.

[6] Lawson, S.A., and Thole, K.A., 2011, "The Effects of Simulated Particle Deposition on Film Cooling," *Journal of Turbomachinery*, **133**(2), pp. 021009-1 – 021009-10.

[7] Albert, J.E., and Bogard, D.G., 2011, "Experimental Simulation of Contaminant Deposition on a Film Cooled Turbine Vane Pressure Side With a Trench," GT2011-46709.

[8] Wammack, J.E., Crosby, J., Fletcher, D., Bons, J.P., and Fletcher, T.H., 2006, "Evolution of Surface Deposits on a High Pressure Turbine Blade, Part I: Physical Characterics," GT2006-91246.

[9] Crosby, J.M., Lewis, S., Bons, J.P., Ai, W., and Fletcher, T.H., 2008, "Effects of Temperature and Particle Size on Deposition in Land Based Turbines," *Journal of Turbomachinery*, Vol. 130.

[10] Webb, J., Casaday, B., Barker, B., Bons, J.P., Gledhill, A.D., and Padture, N.P., 2011, "Coal Ash Deposition on Nozzle Guide Vanes: Part I – Experimental Characteristics of Four Coal Ash Types," GT2011-45894.

[11] Dennis, R.A., Shelton, W.W., and Le P., 2007, "Development of Baseline Performance Values for Turbines in Existing IGCC Applications," GT2007-28096.

[12] Bons, J.P., Crosby, J., Wammack, J.E., Bentley, B.I., and Fletcher, T.H., 2007, "High-Pressure Turbine Deposition in Land-Based Gas Turbines from Various Synfuels," *Journal of Engineering for Gas Turbines and Power*, **129**, pp. 135-143.

[13] Incropera, F.P., Dewitt, D.P., Bergman, T.L., and Lavine, A.S., 2007, "Introduction to Heat Transfer," 5th Edition, John Wiley & Sons, Inc.

APPENDIX E:

Time-Lapsed Video Images of Deposition Growth

The following images show a time lapsed video of the M=0.0 case at 10-15 minute intervals.

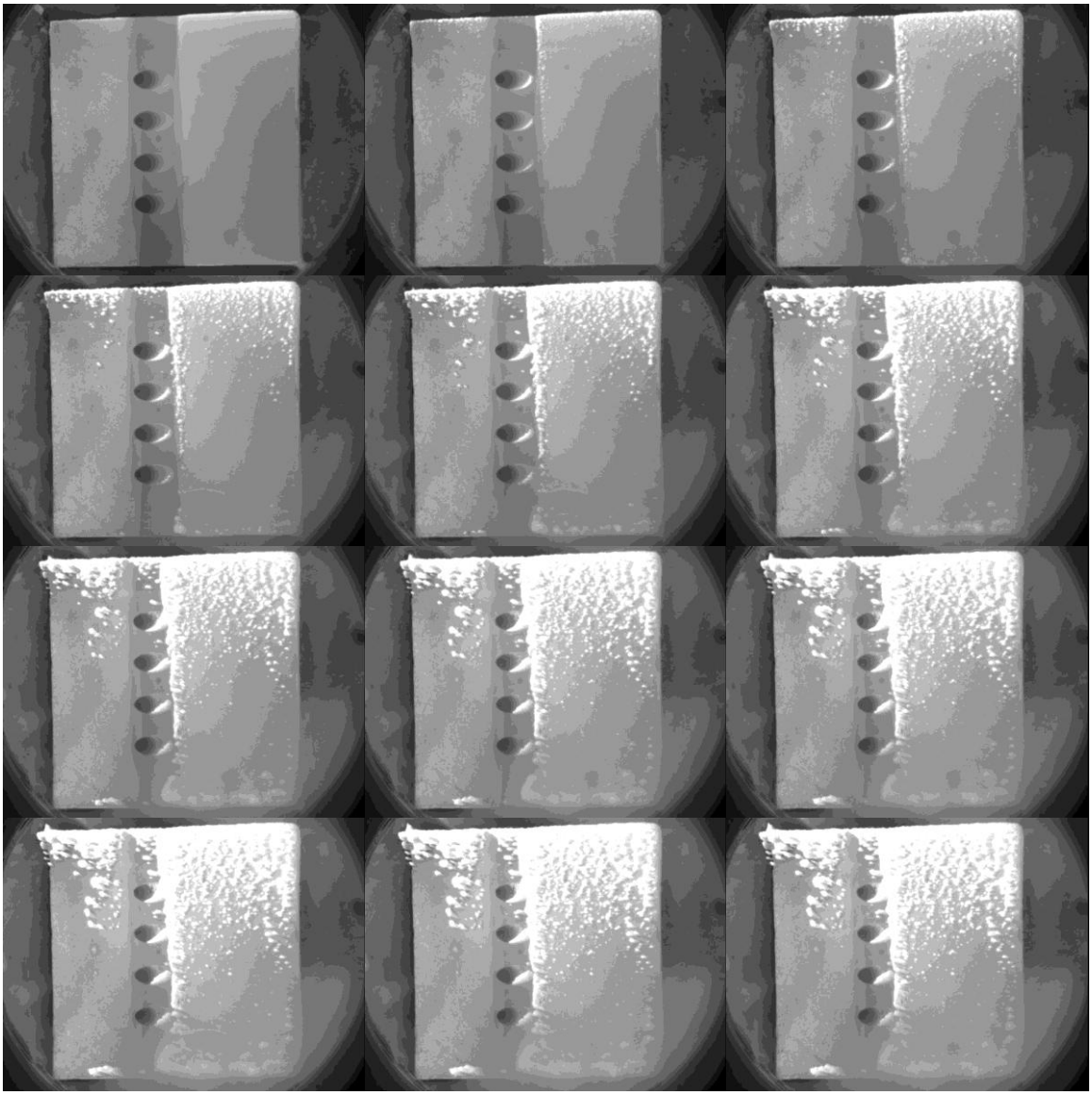

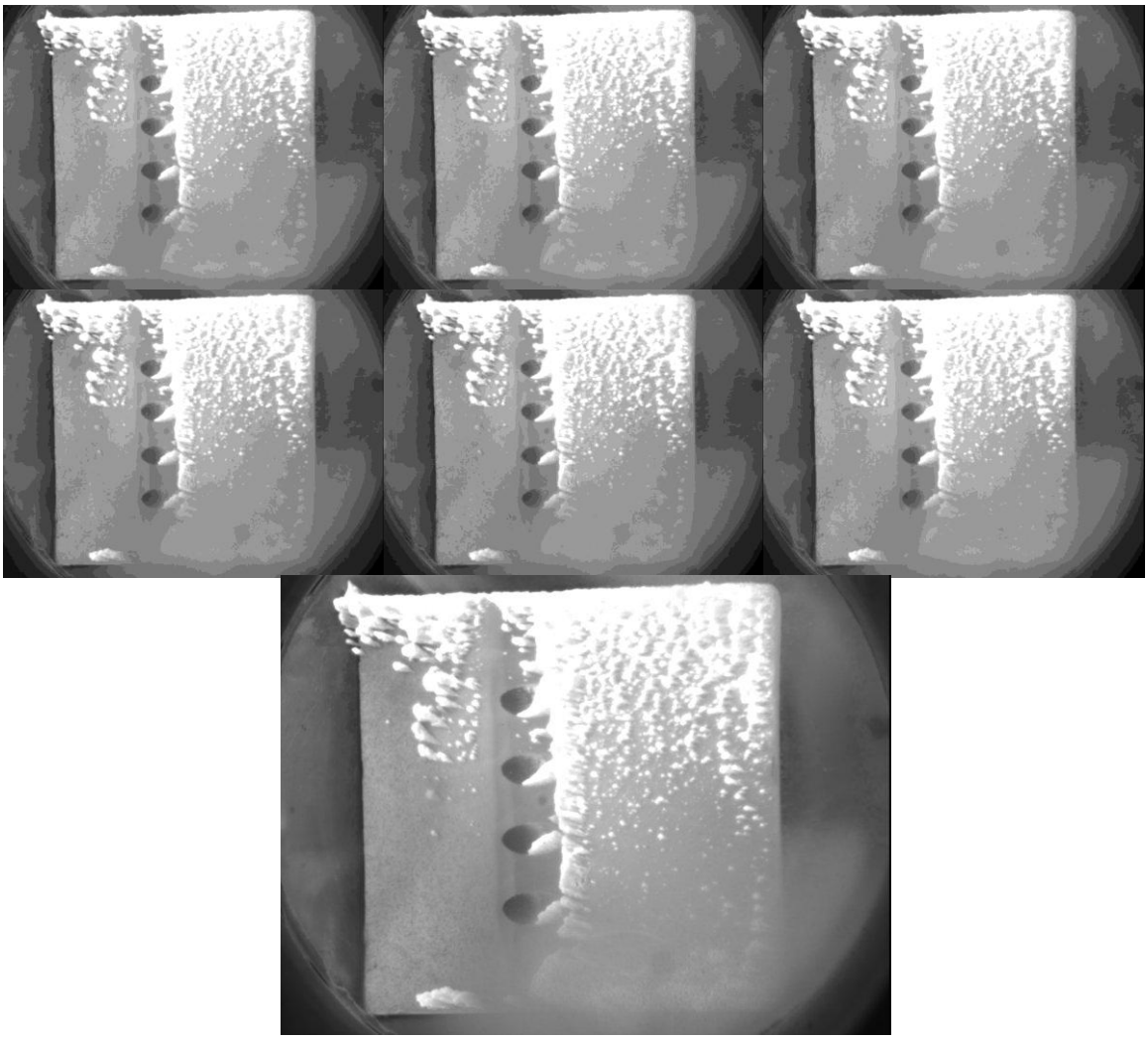

ROBERT G. MURPHY

Mechanical and Aerospace Engineering Department, West Virginia University
Center for Alternative Fuels, Engines and Emissions Tel: 304-237-4590
Engineering Sciences Building Email: rgm4386@gmail.com
Morgantown, WV 26506

EDUCATION

Master of Science in Mechanical Engineering, Mechanical and Aerospace Engineering Department, Benjamin M. Statler College of Engineering and Mineral Resources, West Virginia University, Morgantown, West Virginia. Thesis: *Experimental Investigation Of Particulate Deposition on a Simulated Film-Cooled Turbine Vane Pressure Surface in a High Pressure Combustion Facility*
Chair: Dr. Andrew C. Nix, May 2012

Bachelor of Science in Mechanical Engineering, Mechanical and Aerospace Engineering Department, College of Engineering and Mineral Resources, West Virginia University, Morgantown, West Virginia.

Bachelor of Science in Aerospace Engineering, Mechanical and Aerospace Engineering Department, College of Engineering and Mineral Resources, West Virginia University, Morgantown, West Virginia.

AWARDS

2011 Oak Ridge Institute for Science and Education Fellowship, Energy System Dynamics Group, National Energy Technology Laboratory, Department of Energy, Morgantown, West Virginia.
Mentor: Mr. Douglas Straub

2011 University Turbine Systems Research Fellowship, Heat Transfer Group, Aero, Thermal, and Performance Group, Solar Turbines, Inc., San Diego, California.
Mentor: Dr. Yong Kim

PUBLICATIONS

Murphy, R.G., Nix, A.C., Lawson, S.A., Straub, D., and Beer, S.K., 2012 "Preliminary Experimental Investigation of the Effects of Particulate Deposition on Turbine Film-Cooling in a High Pressure Combustion Facility," (Accepted for inclusion to the 2012 ASME International Gas Turbine Institute Conference, Turbine Heat Transfer Technical Track, Copenhagen, Denmark).

Nix, A.C., Lawson, S.A., and Murphy, R.G., 2012, "Wind Energy Resource Assessment and Power Production Estimates as an Undergraduate Project," (Accepted for inclusion to the 2012 ASME International Gas Turbine Institute Conference, Wind Turbine Technical Track, Copenhagen, Denmark).